國 立 交 通 大 學

電機與控制工程學系

碩 士 論 文

以車道線偵測為基礎之駕駛人昏睡警示安全系統

A Lane-Based Drowsiness Estimation System for Safety Driving

研 究 生：林立倬

指導教授：林進燈 博士

中華民國 九十六 年 七 月

以車道線偵測為基礎之駕駛人昏睡警示安全系統

A LANE-BASED DROWSINESS ESTIMATION SYSTEM FOR SAFETY DRIVING

研 究 生：林立偉　　Student：Li-Juo Lin

指導教授：林進燈 博士　　Advisor：Dr. Chin-Teng Lin

國立交通大學

電機與控制工程學系

碩士論文

A Thesis

Submitted to Department of Electrical and Control Engineering

College of Engineering and Computer Science

National Chiao Tung University

in Partial Fulfillment of the Requirements

for the Degree of Master

in

Electrical and Control Engineering

July 2007

Hsinchu, Taiwan, Republic of China

中華民國 九十六 年 七 月

以車道線偵測為基礎之
駕駛人昏睡警示安全系統

學生：林立倬　　指導教授：林進燈 博士

國立交通大學電機與控制工程研究所

中文摘要

近年來，由於車輛數目的快速成長，造成交通事故問題日益嚴重。在台灣，每年有超過兩千五百人在車禍中喪生。而根據交通部的資料，過去的四年中，每年至少有八萬多件的車禍事故發生。這種情況下促成智慧型運輸系統(Intelligent transportation system, ITS)相關研究的發展越來越受到關注。而大部分車禍發生的原因主要由於駕駛人本身的分心、不注意車況、疲勞駕駛等不適當駕駛行為所引起。因此，為了能盡量避免駕駛者身處於此危險狀態，我們針對車輛後照鏡旁的側邊影像資訊，開發一套以智慧型視覺技術為基礎的車道偵測及偏移系統，以確保駕駛人行駛的安全性。

在車道線偵測部分，為了提高車輛側邊的視角範圍，我們將一支魚眼(Fish-Eye)攝影機架設在後照鏡下方，並利用車體資訊在連續影像中固定的特性，自動選取路面範圍，而不需要事先得知攝影機架設的相關資訊。為了可適用於全天候的光線變化條件，我們同時處理空間及時間軸上的影像資訊，使此系統在白天及夜間人眼可視車道範圍內，都能獲得清晰的車道邊界資訊。另外本論文提出一套分段直線搜尋模組來連結車道線的軌跡，以提升整個搜尋速度，並克服魚眼鏡頭失真的問題。

在車道偏移判斷的部分，本論文利用先前偵測的車道側向位置，及 TLC(Time to Lane Crossing)的瞬時資訊，規劃車道偏移警示的觸發條件。另外建立一個可

以即時更新的車道線位移穩定區間，來模擬駕駛人在直線道路行駛時和車道線保持習慣性距離的特性。最後我們和交通大學腦科學中心(Brain Research Center, NCTU)合作，取得其在虛擬實境動態模擬駕駛系統的環境下，針對駕駛人昏睡狀態預測的相關數據，套用在實際駕駛的影像內容中，使本系統除了估測車道偏移的外在因素外，也可針對駕駛人本身的精神狀況作更進一步的分析，以提升本系統的安全性及可靠性。

本論文發展的車道偵測輔助系統在 1.83GHz 的 PC 平台上平均可達超過 15fps 的執行結果。測試影像內容為在高速公路的實際駕駛環境，並在白天及夜間範圍內都維持穩定的偵測結果。

A Lane-Based Drowsiness Estimation System for Safety Driving

Student: Li-Juo Lin Advisor: Dr. Chin-Teng Lin

Department of Electrical and Control Engineering
National Chiao Tung University

Abstract

As the high growth of population of vehicles, the traffic accidents are becoming more and more serious in recent years. In Taiwan, more than two thousand and five hundred people are died in traffic accidents every year. For each of last four yours, the number of traffic accidents is at least eighty thousand according the statistics of the Ministry of Transportation and Communications (MOTC, R.O.C.). In this situation, a lot of researches about the intelligent transportation system (ITS) have been paid more and more attention to the researches of related fields. Most occurrence of the car accidents results from the distraction, inattention for the adjacent cars, and driving fatigue of the driver. As a result, to avoid the driver being in danger as much as possible, an intelligent vision-based system focused on image contents of lateral-view camera setting under the rear-view mirror on vehicle is developed about lane detection and lane departure warning in this study.

In this thesis of lane detection, a fish-eye camera is located on the vicinity of the rear-view mirror to increase the range of lateral-view angle. Furthermore, we make use of the invariant of image for car body fixed in consecutive image sequences to extract the ROI (region of interest) containing the road surface without realizing the

intrinsic and extrinsic parameters of camera in advance. To make this algorithm suitable for various light conditions all day, the information of image in spatial and temporal domain must be simultaneously processed so that the lane boundary keeps distinct whether people have seen in the day or night environment. On the other hand, a piece-wise line searching model proposed in this paper is to connect the trajectory of lane and to reduce the computation load and to overcome the fish-eye lens distortion.

In the thesis of lane departure warning, the instantaneous information of the lateral position from the result of lane detection and the TLC (time to lane crossing) can be regarded as the warning triggers for the alarms of lane departure. Then, a stable-driving region with real-time update mechanism is constructed to simulate the straight-road driving habit of different drivers which get used to keep approximately the same distance between the vehicle and lane markers. Eventually, by cooperated with the BRC (Brain Research Center, NCTU), we utilize the statistics about drowsiness estimation of the drivers in Virtual-Reality (VR) dynamic driving simulator to implement in the video contents for realistic driving. Therefore, this mechanism can be not only estimated the external factors such as departure of lane boundary but the internal ones such as the conscious analysis of the driver with higher reliability and safety.

The lane detection and departure warning system proposed in this paper has been successfully evaluated on the PC platform of 1.83-GHz CPU with the average frame-rate is up to 15fps. Moreover, this algorithm can be maintained stable results whether in the day or night environment of the realistic driving on highway.

致　　謝

本論文的如期完成，要感謝的人實在太多了。尤其是這兩年的研究生涯，無論是學術上還是生活上的幫助，心中總是對這段時間中曾經在旁陪伴及鼓勵我的人們，保持著滿滿的感激及謝意。

首先要感謝指導教授　林進燈博士的悉心指導，在學術上引導著我走向正確的研究方向。老師同時也給予我很大的空間來盡情發揮想像力及創造力，讓我學習到如何面對及解決問題的正確態度和方法。另外也要感謝傅立成教授、郭耀煌教授不遠千里的來擔任我的口試委員，你們的建議及指教，使本論文的內容架構更為完整。

其次，感謝超視覺實驗室的蒲鶴章、劉得正及范剛維學長，在研究理論及實務上給予我相當多的幫助與建議，讓我獲益良多。也感謝 Vision Group 的博士班學長姊們，及同學亞書、育宏、訓緯及肇廷的相互砥礪，及所有學弟妹們在研究過程中給我的鼓勵與協助。另外感謝腦科學中心鄭仲良同學，提供我很多實驗上的想法及數據參考。以及室友佳華、嘉川、存智在這段時間和我共同度過許許多多難忘的回憶，謝謝你們。

最後要感謝一路走來默默支持我的家人們：我的父母、姐姐、以及哥哥給予我精神及物質上的一切支援，也感謝其他親人對我不斷的關心與鼓勵。特別感謝我的良師兼親友—我的姐夫簡韶逸先生兩年來在研究上給予我許多正確及珍貴的建議。你們的關心及支持，才是我保持研究動力的精神來源。

謹以本論文獻給我的家人及所有關心我的師長與朋友們。

Contents

List of Tables

List of Figures

Chapter 1

Introduction

1.1 Motivation

In recent years, an important social and economic problem is traffic safety. In 1999, about 800,000 people died globally in road related accidents, causing losses of around US$ 518 billion [1]. According to the United Nations, there were more than 23,000 vehicle drivers died in traffic accidents in 2004. The related factors are as listed in Table 1.1[2]. In Taiwan, the number of traffic accidents is increasing in the last years as shown in Table1.2 [3]. In general, a considerable fraction of these accidents is due to driver fatigue, inattentive driving and driving without keeping proper distance. In many cases, the driver falls asleep, making the vehicle to leave its designated lane and possibly causing an accident.

Table 1 : Related factors for drivers involved in fatal crashes.	
Factors	**Percent**
Failure to keep in proper lane or running off road	24.0%
Driving too fast for conditions or in excess of posted speed limit	20.3%
Under the influence of alcohol, drugs, or medication	12.2%
Inattentive (talking, eating, etc.)/ Drowsy, asleep, fatigued, or ill	9.1%
Failure to yield right of way	7.9%
Operating vehicle in erratic, reckless, careless, or negligent manner	6.7%
Others	19.8%

Table 2 : Road traffic accidents and violations in Taiwan from 2001 to 2005.					
Year	**2001**	**2002**	**2003**	**2004**	**2005**
Numbers of Event	64,264	86,259	120,223	137,221	155,814
Fatalities	3,344	2,861	2,718	2,634	2,894
Injuries	80,612	109,594	156,303	179,108	203,087

In order to improve the driving safety, a lot of researches about the intelligent transportation systems (ITS) have been proposed in recent years. Advanced vehicle control and safety system (AVCSS), one part of the ITS, contributes to prevent the driver in danger, and efficiently controls the traffic flow combining the distinct fields of technology, such as sensor, computer, and electrical engineering. Within this paper, we focus on concerning the applications of the smart vehicles. In general, it is so necessary to acquire the information about the lane tendency while driving on the way.

Due to the inattentive driving, the driver may deviate from the correct lane orientation, which induces the traffic accidents. As a result, the lane detection system plays a significant role about improving the driver's safety in moving vehicle. For cost and performance consideration, a camera is chosen as our sensing device so that it can provide more abundant information by consecutive image sequences. Vision-based system with cameras can capture and process the real-time images of road. Many approaches have been proposed about the lane detection algorithm by developing the image processing. More explanation of their techniques will be introduced in the next section.

1.2 Background

1.2.1 Previous Works of Lane Detection

The ARGO system [4] proposed at the University in Parma, Italy is aimed to develop the autonomous vehicle that could drive on highways and rural roads. In the GOLD system [5], the IPM (inverse perspective mapping) architecture was constructed to remove the perspective effect by mapping the road image into the top

view. Moreover, this algorithm can detect the lane markings depending on the feature of the contrast and lane-width with the road plane, which may fail when the assumption of a flat road is not valid. Based on the GOLD system, Jiang et al. [6] model the lane as two straight lines to estimate the inclined angel on the degree of non-flat roads. However, the road shape is not usually straight in realistic conditions. Based on the lane geometry, some geometric model-based lane detection techniques such as polynomials and splines can fit the lane trajectory more than the model of straight lines. Y. Wang and E. K. Teoh [7] [8] have proposed the deformable road models to track the lane curvature without any camera's parameters. But The searching speed of those correlated methods is slower while finding the new control-point in each frame. C. R. Jung [9] has developed the parabolic lane boundary model to approximate the lane boundaries by the combination of the edge function. This technique only demands the low computational power but has difficulty in porting on other platform except for the PC due to the fitting process. To extract the lane shape in the nighttime, L. C. Fu [10] used the vision-based driver assistance system to enhance the driver's safety at night with the preprocessing of camera calibration.

1.2.2 Previous Works of Lane Departure Warning and Driver Analysis

The lane departure warning system issues an alarm to arouse driver's attention and reduce the seriousness of an accident. In general, some algorithms have been developed to predict when the driver is departing the road by the lateral offset or TLC (time to lane crossing). Risack et. al [11] used both vision and radar-like information

to estimate TLC. Kim and Oh [12] proposed a driver adaptive LDW system based on fuzzy techniques. Volkswagen researchers [13] used several sensors (radar, vision and laser) to detect lane shifts. Enkelmann [14] has simultaneously considered the gear angle, lane width, and lateral velocity of the car to clearly determine when a departure warning should be given without the intentional driving behavior.

The trigger of the LDW alarm must not only prepare adequate time in advance for the driver to respond to a truly dangerous situation but reduce the number of nuisance alarms caused by the driving habits of different individuals. Batavia [15] has been proposed a driver-adaptive system with a memory based learning framework for driver analysis. Based on the negative behavior adaptation of the human driver, the dynamic assistant policy has been combined with the LDW system by studying in the fixed-based driving simulator to adapt various driving style and raise the safety [16].

1.3 Objective

To avoid the driver being in the presence of the hazards due to the distracted mentality and expand his/her field of lateral view while driving at high speed, the vision-based lane detection and departure warning system are developed by mounting the fish-eye camera under the rear-view mirror of the vehicle. Without the intrinsic or extrinsic information of the camera in advance such as some previous measures for lane-boundary extraction, the algorithm is developed to automatically search for the ROI (region of interest) on the road plane only by the information of image sequences. The disadvantage of the image sensors is sensitive to various illumination factors even in the nighttime. However, the chances of traffic accidents are easily raised in

foregoing situation because of the driver's unclear sight. The objective of our proposed system is to work normally whether the light conditions change a lot or not.

Another important problem is that the vehicle is departing from its own lane without keeping the proper lateral velocity along with the risk of the driver's life. To prevent the vehicle from being too close to or far from the lane, the lateral position and velocity of the lane boundary are the key factors to predict when the departing action occurs as soon as possible. Furthermore, by the related information of the lateral view computed by the above mechanism, this system can be incorporated into the driver analysis method to avoid the frequently incautious behavior of the driver, especially for the straight-road driving on the highway.

1.4 Organization

This thesis is organized as follows. In Chapter 2, the camera configuration and the vehicle blind-spot is introduced along with the preliminary knowledge of the vision-based system. Chapter 3 describes our algorithm of lane detection. The approaches about lane departure warning and drowsiness prediction of the driver are proposed in Chapter 4. The experimental results are exhibited in Chapter 5. Finally, the conclusions of our system are presented in Chapter 6.

Chapter 2
Preliminary

In this chapter, the preliminary knowledge of the whole system will be introduced. In the beginning, the difference of the visual characteristics between the frontal and lateral place mounted on the camera is discussed. Then, the vehicle's blind spot based on the intrinsic and extrinsic limitation of the human and rearview mirror will be described. The related principles of the lane detection and departure warning system are presented finally.

2.1 Camera Configuration

In this section, the geometric relationship and transformation between the image coordinate and the realistic vehicle coordinate are explained in detail. Furthermore, the applications about the frontal and lateral view of the camera are introduced here.

2.1.1 Perspective Geometry

To extract the image information of road plane on the side of the vehicle, a single camera is mounted near the rearview mirror. In the vision-based configuration, each objects captured by the image sensor in the camera coordinate system can be projected onto the image pane in the image coordinate system. This geometric relationship can be described as the perspective projection, and the camera configuration for the proposed system is shown in Figure 2-1 with the height of the camera H and the tilt angle α .

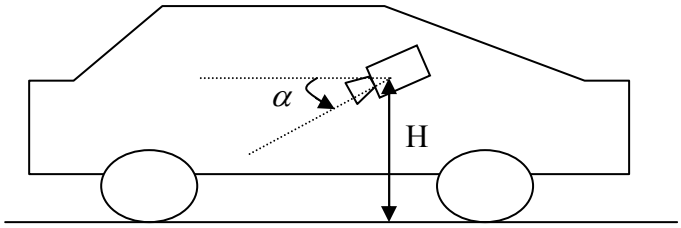

Fig. 2-1 : Camera configuration.

Before computing the transformation between the image coordinate and the vehicle coordinate, some assumption must be established. At first, the condition in this section is only considered that the ground plane is almost flat. In general, we ignore the specific environment when the vehicle drives on the mountain road or other rugged surface. Second, the optical distortion of the camera lens can not be considered in this deduced process of the geometric transformation.

The spatial relationship between the vehicle coordinate and image coordinate system are shown in Figure 2-2. For practicality, the pan and tilt angle of the camera must be taken into account for this systematic configuration. The tilt angle α is an included angle from road plane to the optical axis. On the other hand, the pan angle β is an included angle from the moving direction of the vehicle (Y-axis) to the projection of the optical axis onto the road plane. In general, the camera can be modeled as the pin-hole model. The distance between the optical center (OC) and the central point of the image plane (u_0, v_0) determines the focal length. Moreover, according to the known camera height H and the information of pan-tilt angle, we can deduce where the object contained by the road surface are projected onto the image plane from the perspective geometry.

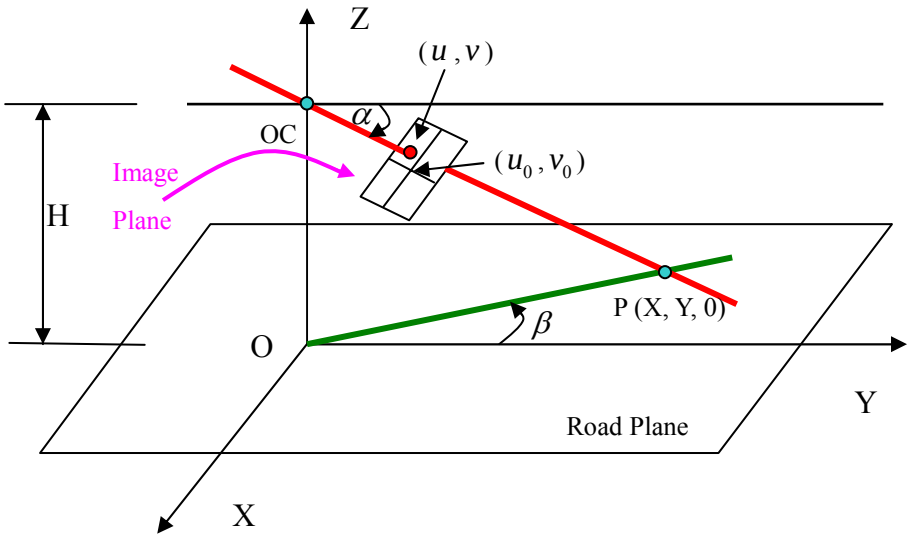

Fig. 2-2 : Vehicle and image coordinate systems.

For further analysis, we discuss the spatial relation between the vehicle coordinate and the image coordinate system through two different points of view. Figure 2-3 and Figure 2-4 are the side view and bird's eye view of the geometric chart between the vehicle coordinate and the image coordinate system.

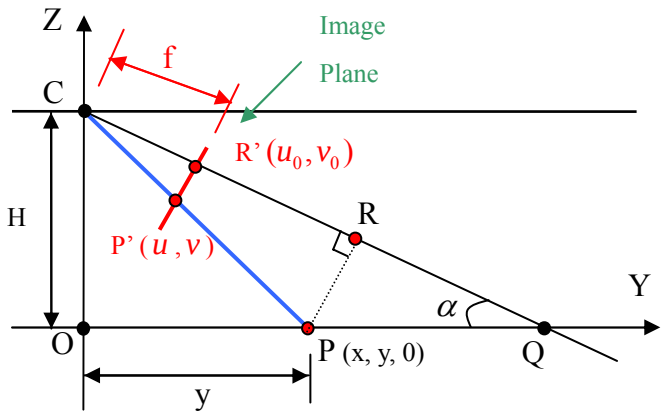

Fig. 2-3 : Side view of the geometric relation between the vehicle coordinate and the image coordinate system.

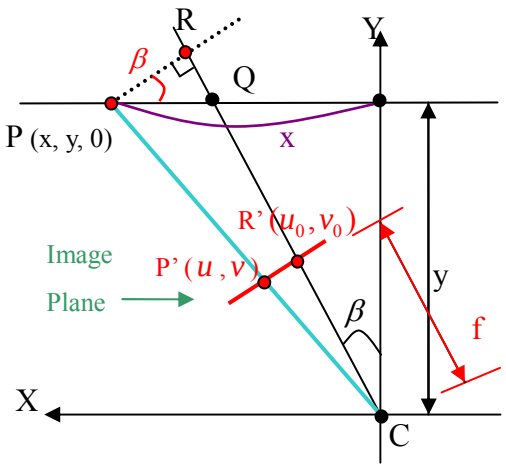

Fig. 2-4 : Bird's eye view of the geometric relation between the vehicle coordinate and the image coordinate system.

Before explaining the formulation of the transformation between the two coordinate systems, some annotation must be introduced about Fig. 2-3 and Fig. 2-4 in advance.

f: Focal length of the camera

f_u 、 f_v : The scaling factors of the image plane in the horizontal and vertical axis

H: The distance from the road plane to the camera

α : Tilt angle of the camera

β : Pan angle of the camera

(u, v): The corresponding point in the image plane is projected from the road surface

(u_0, v_0) : The central point of the image plane

In Fig. 2-3, ΔCPR and $\Delta CP'R'$ are similar triangles. With this property, the spatial relation between two coordinate systems can be derived as follows.

$$\frac{\overline{PR'}}{\overline{CR'}} = \frac{\overline{PR}}{\overline{CR}}$$

$$\Rightarrow \frac{(v-v_0)\cdot f_v}{f} = \frac{\overline{PQ}\cdot\sin\alpha}{\overline{CQ}-\overline{PQ}\cdot\cos\alpha} = \frac{(\frac{h}{\tan\alpha}-y)\cdot\sin\alpha}{\frac{h}{\sin\alpha}-(\frac{h}{\tan\alpha}-y)\cdot\cos\alpha}$$

$$\Rightarrow \frac{(v-v_0)\cdot f_v}{f} = \frac{h\cdot\cos\alpha - y\cdot\sin\alpha}{\frac{h}{\sin\alpha}-(\frac{h\cos^2\alpha}{\tan\alpha}-y)\cdot\cos\alpha} = \frac{h-y\cdot\tan\alpha}{h\cdot\tan\alpha+y}$$

$$\Rightarrow [f_v\cdot(v-v_0)+f\cdot\tan\alpha]\cdot y = [\tan\alpha\cdot f_v\cdot(v-v_0)-f]\cdot h$$

Assume $S_v = \frac{f}{f_v}$ is the camera constant of the image plane in the vertical axis

$$\Rightarrow y = \frac{[(v-v_0)\cdot\tan\alpha - S_v]\cdot h}{(v-v_0)+S_v\cdot\tan\alpha} \tag{2-1}$$

Similar to the above process, the deducing details about Fig. 2-4 will be described in the following.

$$\frac{\overline{PR'}}{\overline{CR'}} = \frac{\overline{PR}}{\overline{CR}} = \frac{\overline{PQ}\cdot\cos\beta}{\overline{CQ}+\overline{PQ}\cdot\sin\beta}$$

$$\Rightarrow \frac{(u-u_0)\cdot f_u}{f} = \frac{(x-y\cdot\tan\beta)\cdot\cos\beta}{\frac{y}{\cos\beta}+(x-y\cdot\tan\beta)\cdot\sin\beta} = \frac{x\cdot\cos\beta - y\cdot\sin\beta}{y\cdot\cos\beta+x\cdot\sin\beta}$$

$$\Rightarrow \frac{(u-u_0)\cdot f_u}{f} = \frac{x-y\cdot\tan\beta}{y+x\cdot\tan\beta}$$

Assume $S_u = \frac{f}{f_u}$ is the camera constant of the image plane in the horizontal axis

$$\Rightarrow \frac{u-u_0}{S_u} = \frac{x-y\cdot\tan\beta}{y+x\cdot\tan\beta}$$

$$\Rightarrow x = \frac{y\cdot[(u-u_0)+S_u\cdot\tan\beta]}{S_u-(u-u_0)\cdot\tan\beta} \tag{2-2}$$

Equation (2-1) and (2-2) are the transformation from the point (u, v) in the image plane to that (x, y, 0) within the road surface in the vehicle coordinate system. However, parts of the parameters in this formulation are unknown. We must make use of some probable approach to estimate those values if the precision of the perspective

phenomenon is adequate.

2.1.2 Applications of Frontal-View Lane Detection

For several years, many researchers worked on driving assistance problem by using the concept of artificial vision. Among those applications about intelligent transportation, automatic navigation has been taken seriously in recent years. For accomplishing this objective with efficient performance, most vision-based methods are to extract the road information by mounting the image sensor on the windshield of the vehicle. Such as the human eye, forward-looking camera can extract the widest field of view than other mounting position around the car body. In general, by detecting the contrast between the white lines and the road, the lane boundary in front of the vehicle can be sufficient to detect. Furthermore, the variation of the lane's curvature can be predicted in time without resulting in the erroneous following of the vehicle. Besides, some obstacles captured by the camera can be recognized with 2D or 3D techniques of computer vision. Other related works such as keeping the secure distance ahead of the car are based on this system configuration.

2.1.3 Applications of Lateral-View Lane Detection

Some risks of road traffic which occur on highway during the lane-changed maneuver happen easily if another vehicle besides the own one has been overlooked. In other words, drivers have not assured accurately if there is no other vehicle alongside in the blind spot of the lateral view. During the general driving procedure, drivers must keep notifying the frontal field of view so that they forget to check the information of the lateral blind-spot at the same time. In order to overcome this kind

of traffic hazard with efficiency, a camera is mounted at the driver's outside rear-view mirror to monitor the blind spot and the alongside lane. Approaching vehicles should be detected in time and tracked until they leave the blind spot by this configuration. In addition, this system can restrain the intended lane -changed maneuver and maintain the distance from the lane boundary in the blind spot to the realistic car body without a significant amount of the potential collisions.

2.1.4 Comparison with Two Applications on Vehicle

In addition to the distinct effect of the geometric projection onto the image plane, there are still other different factors and applications between the frontal-view and lateral-view configurations. The four reasons are listed as follows.

(1) The initial purpose has influence on where the camera is mounted:

As explained in section 2.1.2 and 2.1.3, road images extracted from the forward sight of the vehicle can yield more driving information to track the real-time road curvature by the lane-marking modeling. Furthermore, the related data of them has effectively contributed to the system with respect to the assistant navigation. On the other word, the major objective about mounting the camera on the side of the car is to adjust how much is the detecting range of the blind-spot region. This configuration only puts emphasis on judging the approaching car or the lane trajectory near the vehicle, and the variation of the forward road information can be not considered.

(2) The diverse sensation of the driver with respect to two mounting position:

In general, to extract the forward visual information as far as possible, the camera was almost fixed to the windshield. This setting location could easily reduce the eyesight of the driver whether the size of the camera is so small or not. The

disadvantage resulting from the driver's unfamiliar looking will be concerned with the research about driver analysis. Nevertheless, due to the position of the camera near the rear-view mirror when focusing on extracting the lateral-view content of the vehicle, drivers can be not confused with this experimental environment. In other words, the camera added to the vehicle can not affect the original driving habit of the driver, and the data collected by driver analysis system will still be higher accuracy.

(3) The different extrinsic factors of two locations of the sensing device

Compared with the initial purpose of two configurations, the camera mounted in front of the vehicle must have farther distance from its optical center to the specified lane portion on the road plane than that on the side of the car because of the perspective geometry. In addition, the overtaking cars which crossing the lane are almost captured by the frontal-view image sequences. Therefore, the information of the lane trajectory extracted by the sideward camera can be more complete than the forward one throughout the driving experiment on highway. However, with the headlight switched in the gloomy driving situation, the video collected by the frontal camera can still hold more acceptable luminance information in night vision.

2.2 Definition of Vehicle Blind Spot

Blind spots, in the context of driving an automobile, are the areas of the road that cannot be seen while looking forward or through either the rear-view or side mirrors. Detection of vehicles or other objects in blind spots may also be aided by systems such as video cameras or distance sensors. Throughout the notation in this thesis, the

area of blind spot is only regarded as the rear of the vehicle on both sides. The introduction in this section not only describes the causes of traffic accidents resulted from the blind spot, but discuss how to resonablely establish the region of blind spot by the inherent limitation of the human vision and rear-view mirror.

2.2.1 Traffic Accident Causes of Vehicle Blind Spot

In Taiwan, the types of traffic accidents between two cars on highway are listed in Table 2.1 from [17].

Table 3 : Causes of traffic accidents between two cars on highway.

Year	Collision by the Backward Car	Rubbed Collision in the Same Direction	Lateral Collision	Colliding Collision	Others
2001	59.74%	28.57%	2.86%	1.56%	7.27%
2002	62.39%	28.04%	3.04%	1.74%	4.78%
2003	60.82%	27.88%	3.70%	2.34%	5.26%

As shown in foregoing statistics, we can conclude that the lateral and rubbed collisions are both the principal causes of the traffic accidents between the cars. There have been numerous topics focused on how to avoid the forward or backward collision for the vehicle, but the related research for lateral collision is little. When vehicles in the adjacent lanes of the road fall into the range of lateral blind spots, the driver will be unable to see them with only the car's mirrors. Due to the above reason, drivers must actively rotate their head to extract more information within the region of blind spot. However, the probability of car accident can be raised simultaneously. Therefore, vision-based system can be developed to assist the drivers in keeping away from the lateral danger of vehicles by the image sensor alongside the rear-view mirror.

2.2.2 Limitation of View by Human-Vision

The eyesight of people has obvious difference between the static and dynamic environment due to the variation of the vehicle velocity. In general, the view-angle of the single eyeshot is about 160 degrees when people lie in the stationary scene; the maximum view-angle of the double field of view is enlarged about 180 degrees. Flannagan [18] proposed that the people's double eyesight should reach to 320 degrees by adding the rotating motion for the head and body of human. According to the statistics from [19], the realistically clear field of view contained two eyes is only about 70 degrees when a normal person situates in the static environment. Nevertheless, the human's eyesight could frequently vary when people are in the dynamic conditions such as the internal part of the moving vehicle thanks to the tunnel-vision effect. The relationship between the range of human eyesight and the variation of the vehicle velocity is in Table 2.2; the range of field of view between the static or dynamic environment is shown in Fig. 2.5.

Table 4 : The relationship between the field of view and the vehicle velocity.

Speed (km/hr)	**40**	**70**	**100**
Field of View (degrees)	100°	65°	40°

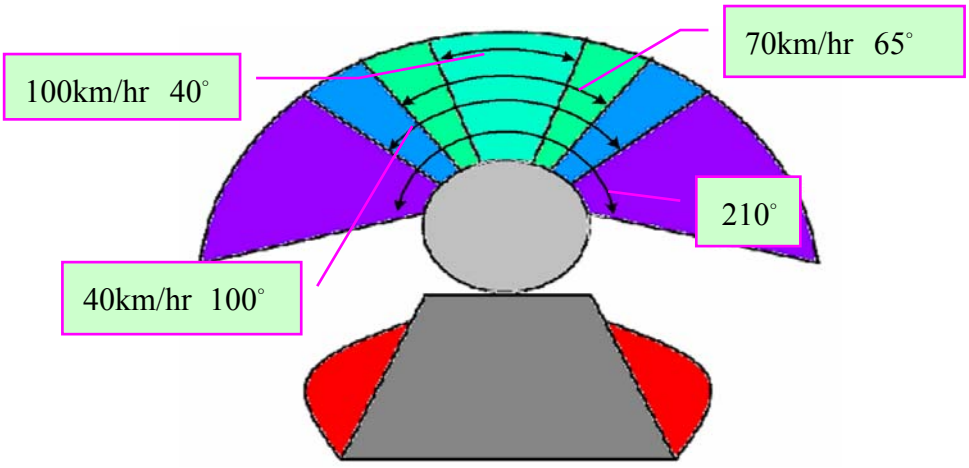

Fig. 2-5 : The diagram of the driver's field of view.

As the information shown in Fig. 2-5, the eyesight becomes greatly narrow when the vehicle is driven at high speed. In other words, the driver can not judge whether there are other vehicles moving on the adjacent road surface or not only by his/her remaining eyeshot on highway as the car velocity raises to 100 km/hr. In this way, drivers induced by the blind-spot hazard will be easily in danger.

2.2.3 Limitation of View by Rear-View Mirrors

In general, the side mirrors of the vehicle are almost used by the planar type. Therefore, the formation of image about the normal rearview mirror is still followed by the principle which describes that the angle of incidence (θ_i) is the same as that of reflection (θ_r). In other words, the field of image produced by the rearview mirror is stretched to 2θ ($\theta=\theta_i=\theta_r$) view-angle projecting into the road surface.

The relationship between the field of view of the side mirror and that of the driver is shown in Fig. 2-6.

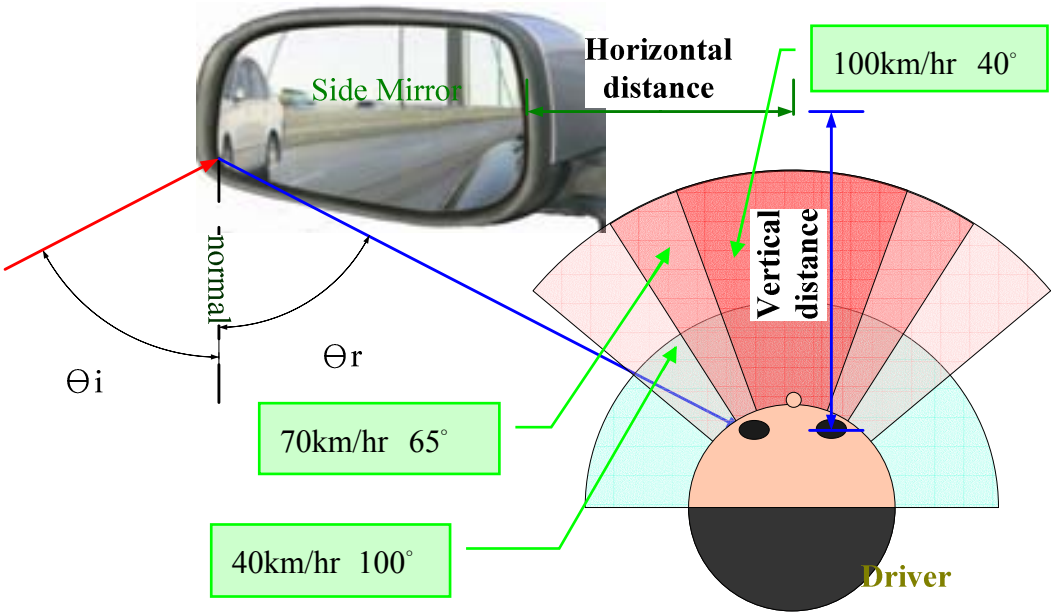

Fig. 2-6 : The relation about field of view between the side mirror and the driver.

By the geometric relation from Fig. 2-6, when driving at high speed, in order to make the eyesight overlap the reflected field of rearview mirror, the driver must rotate his/her head so as to extract the lateral information as much as possible. However, due to this unnatural motion, the driver's inattention will not keep his/her eye for the forward state of the vehicle for a long time with the occurrence of traffic accident.

There are two general approaches to extend the range of field of the rearview mirror. The first approach is to increase the distance between the side mirror and the driver. Due to the fixed car-body, this improving effect will be restricted. The second approach is to replace the traditional planar mirror with the curved one. Nevertheless, the distortion effect of the reflected image will be serious due to the curvature of the lens. Through the above discussion, the blind-spot region between the side mirror and the driver can not be easily resolved. For this reason, adding the camera on the side of the car with intelligent vision-based algorithm will still be regarded as the important device of the assistant system for the driver's safety.

2.3 Principles of Lane Detection

The objective of lane detection method we expected in this thesis is to extract the lane markers without knowing the internal or external parameters of the camera alongside the vehicle in advance. Besides, the sensitivity of the image sensor easily disturbed by the light condition must be suppressed as much as possible. Therefore, developing an adaptive lane-finding system is essential to satisfy the previous demands. First, our system can automatically extract the ROI contained by the road surface only by the image content despite the unknown environmental information of camera. Second, the preprocessing tasks will be able to effectively restrain the noise when driving in the nighttime. Through the property for the view-angle of blind spot, the improving edge operator will be added to acquire the clear lane boundary. Not depending on the distortion of the camera lens which results in the obviously curved lane trajectory even if people drive on the straight road, a piece-wise edge linking model will be developed to mark all information of lanes shown in image sequence.

2.4 Principles of Lane Departure Warning and Drowsiness Prediction

The part for lane departure warning is to provide some triggers for caution with respect to the driving-off-road behavior through the lateral information of the lane extracted by the lane detection algorithm. After measuring the lateral velocity from the consecutive frames, the warning system will determine when the departure driving occurs based on the lateral displacement and TLC (time to lane crossing.)

On the other hand, the part for drowsiness prediction will try to combine the

experimental results of BRC (brain research center) from NCTU with the realistic driving video. In order to estimate the lateral location of lane where the driver gets used to navigate on the straight road, we construct the single Gaussian model to simulate the stable-state range about the lane position. Then, the additional updating mechanism will contribute to the systematic adaptation even if the driver changes his/her driving habits. At last, the proportional gauge of the drowsy degree we proposed will show if the driver has higher or lower probability in the drowsy state at that moment with the amount of reflection time measured by the lane position over the stable-state region.

Chapter 3

Lane Detection

3.1 Overview

Figure 3-1 shows the flow chart of lane detection. At the beginning of this architecture, because we merely aim at the monochromatic information of each frame to process, the RGB coordinate will be transformed into the YCbCr one so that the illumination component will be totally retained. Then, the automatic mechanism about searching the ROI (region of interest) of the image content will be described in Section 3.2.1. The preprocessing step about de-noising will be presented in Section 3.2.2.

Next to the processing step, the flow will enter the principal detection parts. Due to the mounting position of camera on the side of the car, the image captured by that device will contain most of the lateral-view information next to the wheels. In other words, only one lane trajectory which is the most closed to the vehicle can be apparently seen. An edge detection operator will be developed to adapt to the geometry relationship of the camera based on the property of view-angle in Section 3.3. In addition, the binarization step we proposed in this section will depend on the spatial relation with respect to the perspective effect. To eliminate the blind-spot region as much as possible, we choose the fish-eye camera for enlarging the field of view with some obvious distortion result. Therefore, the adaptive edge-linking model demonstrated in Section 3.4 will overcome the serious problem whether the lane boundary in the image sequences is straight or not.

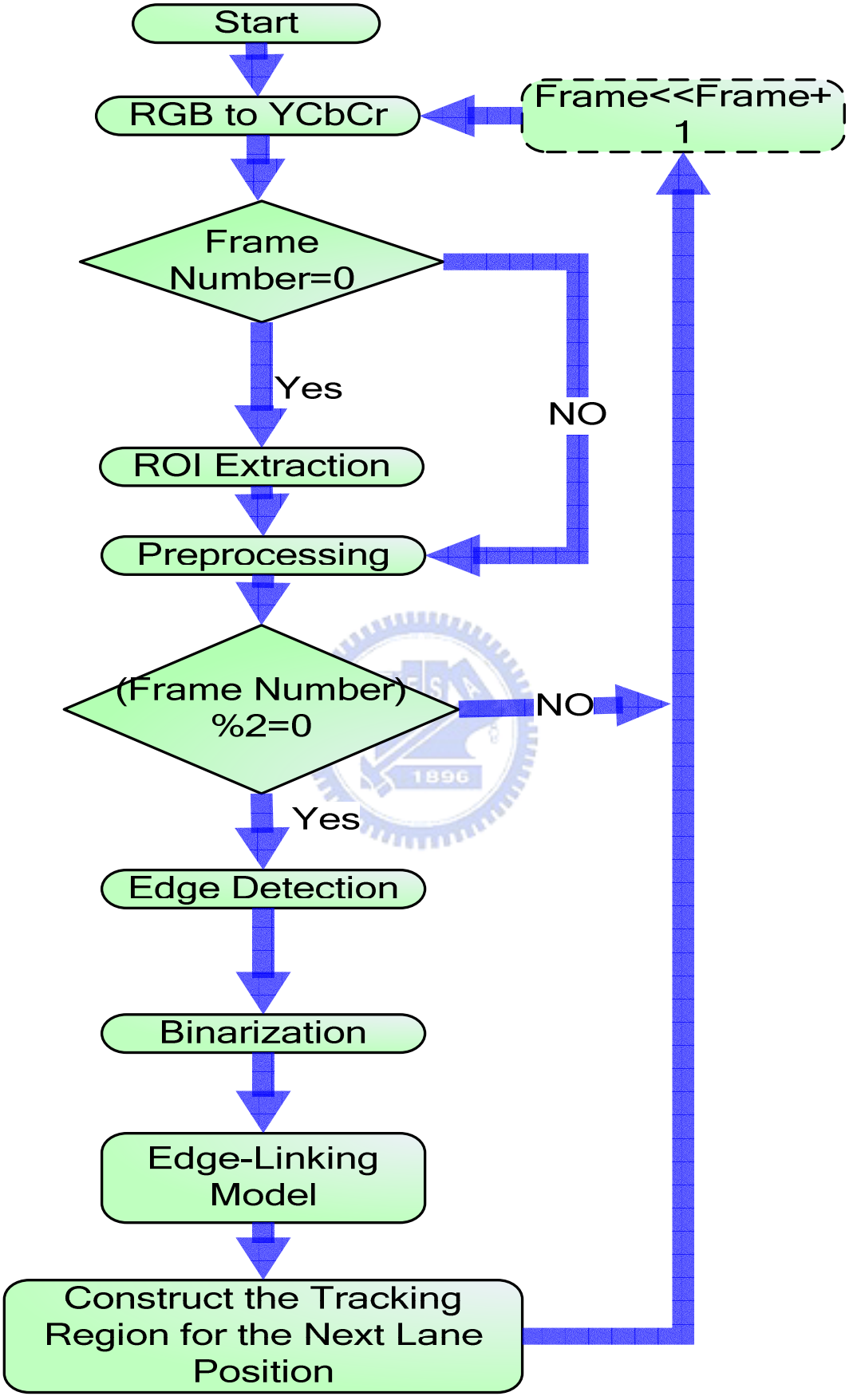

Fig. 3-1 : The flow chart of lane detection.

3.2 Preprocessing

3.2.1 Automatic ROI Extraction

Before discussing how to search for the lane-marking, the step of color transformation must be executed. In general, most of the algorithms shown in the past theses with respect to lane detection are only considered the grey-level component. This reason is that the contrast between the lane boundary and the normal road plane can be easily seen by normal people as usual even if the colors of lanes are not necessarily the same. As a result, the information of luminance for each frame must be stored in our system by the RGB-to-YCbCr transformation. On the other hand, the remaining chrominance components such as Cb and Cr are not taken seriously due to the insensitive perception about human eyes. The formulation of transformation can be described by

$$\begin{bmatrix} Y \\ Cb \\ Cr \end{bmatrix} = \begin{bmatrix} 0.257 & 0.504 & 0.098 \\ -0.148 & -0.291 & 0.439 \\ 0.439 & -0.368 & -0.071 \end{bmatrix} \cdot \begin{bmatrix} R \\ G \\ B \end{bmatrix} + \begin{bmatrix} 16 \\ 128 \\ 128 \end{bmatrix} \tag{3.1}$$

As shown in Section 2.1.1, equation (2-1) and (2-2) tell us the relationship of geometric transformation which demands the known information of camera, such as the height, pan-tilt angle, and the internal focal-length of the camera, between the image coordinate and the vehicle coordinate systems. Some methods proposed in the previous works have to compute the curvature of the realistic road plane or to estimate the lane shape effectively by these intrinsic or extrinsic parameters. However, an adaptive system can not be sensitive to the variation of the camera mounting position for the aspect of application and commerce. For instance, the systematic performance

should be not influenced by the distance between from the rear-view mirror and the road surface about various vehicles.

To take this target, we hope that our detection algorithm can automatically determine the ROI (region of interest) contained the whole lane trajectory on the road surface only by the image content with lateral view-angle. The chosen range of ROI should be unchanged by the later information of image sequences whether some new moving objects are captured or not. Figure 3-2(a) demonstrates the realistic frame acquired by the camera alongside the side mirror. Through being concerned about the image content, the fixed parts within it might be regarded as the evidence for ROI extraction. In our opinion, the sideward car body with constant area throughout the image sequences and the horizon relative to the road plane both correspond to the fixed condition. Therefore, the approximately location of ROI will be determined by the edge information of them.

The definition of ROI is that a rectangle region which extends its width to the location next to wheels contains all the lane shapes in the image. In general, the height of ROI is below the vanishing point situated in the horizon closed to the border of vehicle's window. This 2D geometry with respect to the above characteristics can not depend on the light condition or view-angle of the camera.

(a) (b)

Fig. 3-2 : (a) The image acquired by the camera alongside the rearview mirror. (b) The upper left point of ROI next to the boundary of the vehicle window.

Figure 3-2(b) shows the location of the upper left point of ROI between the boundary of the window and the vanishing point. In this figure, the portion of green rectangle is shown as ROI, and the intersection of the marking cross stands for the key point to determine where the range of ROI has covered. In this case, the 2-D gradient operator will be used to extract the position of key point by considering the boundary information of the vehicle window. Hence, we use only two of eight-directional Sobel masks for detection due to the obvious edge of the window in the horizontal and vertical aspects, as follows:

x, y : coordinate values of each pixel in the x and y axis

f (x ,y) : the intensity of this pixel

$$G_x = [f(x-1,y+1)+2\cdot f(x,y+1)+f(x+1,y+1)]-[f(x-1,y-1)+2\cdot f(x,y-1)+f(x+1,y-1)] \quad (3.2)$$

$$G_y = [f(x-1,y-1)+2\cdot f(x-1,y)+f(x-1,y+1)]-[f(x+1,y-1)+2\cdot f(x+1,y)+f(x+1,y+1)] \quad (3.3)$$

-1	-2	-1
0	0	0
1	2	1

(a)

1	0	-1
2	0	-2
1	0	-1

(b)

Fig. 3-3 : The mask type of (a) G_x . (b) G_y .

The two mask types are shown in Fig. 3-3. Figure 3-4 displays the results of Sobel edge detection with Gx and Gy. After extracting the border of the window from Fig. 3-4 (b) to Fig. 3-4(d) with thresholding, the coordinate values of the key point in the x- and y- axis will be founded to determine the range of ROI by computing which row and column retain the most edge pixels along the horizontal and vertical direction individually. This process can be expressed as:

$$I_{key}(x,y)=\begin{cases}255 & \text{if } G_x(I(x,y))>TH \text{ or } G_y(I(x,y))>TH \\ 0 & \text{else}\end{cases} \tag{3.4}$$

where

$$TH=\frac{\sum_{y=0}^{h}\sum_{x=0}^{w}I(x,y)}{w\cdot h} \tag{3.5}$$

The ratio of w to the image width is closed to 0.5, and that is the same case as the ratio of h to the image height. Due to the more edge pixels naturally existed along the horizon in the horizontal axis and the perpendicular border of vehicle in the vertical axis, an intersection point of the car window can be found out by searching in the x-y direction respectively. The detecting results with different light conditions and view-angles are shown in Fig. 3-5.

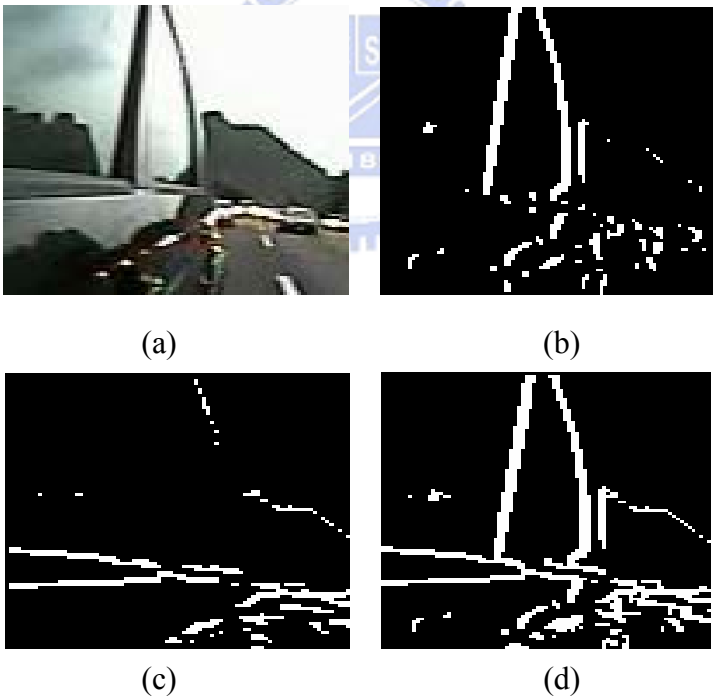

(a) (b)

(c) (d)

Fig. 3-4 : (a) Original image. (b) Edge detection by Gy. (c) Edge detection by Gx. (d) Edge detection by Gx+Gy.

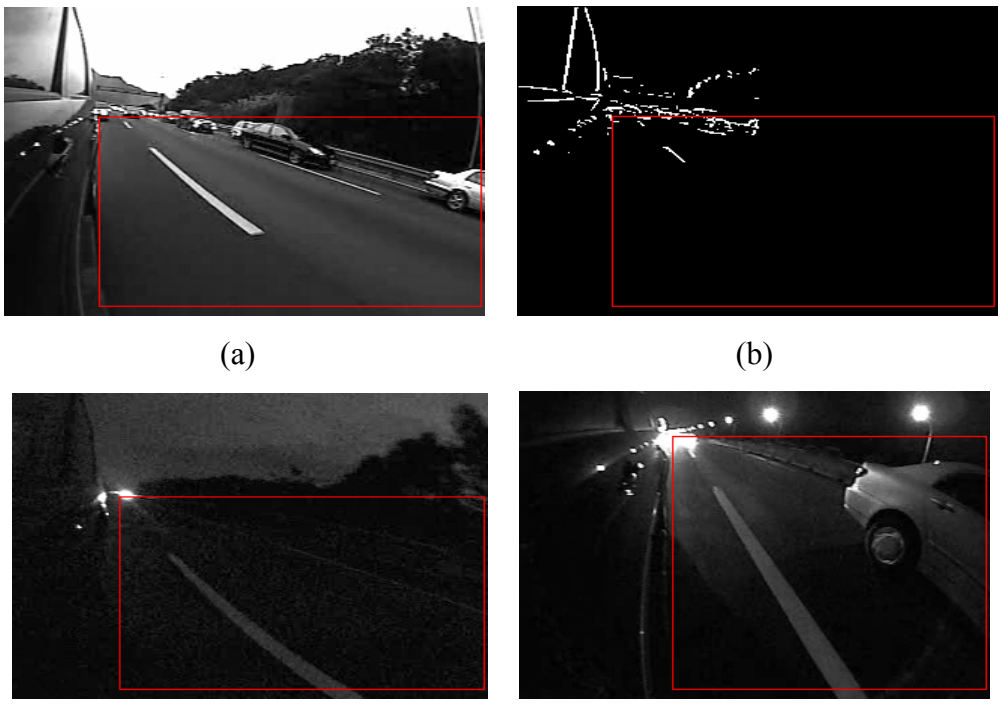

(a) (b)

(c) (d)

Fig. 3-5 : (a) Day light. (b) ROI extraction of (a). (c) ROI extraction at night. (d) ROI extraction with different view-angle in the nighttime.

Although the horizontal border of vehicle window may be unclear in the worst conditions which the illumination from the car and street light has not adequate at night, the extracting result is still steady since the edge information of horizon can be replaced to obtain the similar position in the x-axis, as shown in Fig. 3-5(c) and (d).

3.2.2 De-noise Processing in Spatial and Temporal Domain

The quality of image sequences collected by the vision-based sensing device will be almost subjected to this challenge of the variance of light conditions, such as day or night situation. Because the problems about high-frequency noise will be serious for some driving environment due to the photosensitivity of cameras, especially on

night vision. Therefore, the preprocessing step for eliminating the noise effect must be considered in the detecting architecture if the system is expected to work robustly all day long.

In general, a low-pass filter can be implemented before the process which is used to extract the information about the boundary, texture, or shape of the interesting objects within the frame. Since the frame is stored as a collection of discrete pixels, we need to produce a discrete approximation to the chosen filter-type before the convolution step. Hence, the Gaussian smoothing operator which is a 2-D point-spread function achieved by convolution is used for this de-noising task in our system. The isotropic form of Gaussian is shown as below:

$$G(x,y)=\frac{1}{2\pi\sigma^2}\exp(-\frac{x^2+y^2}{2\sigma^2}) \tag{3.6}$$

where σ is the standard deviation of this function

The diagram of this distribution is shown in Fig. 3-6(a). Moreover, this function has been assumed with a zero mean. In principle, the Gaussian distribution is non-zero everywhere, but its value is closed to zero more than about three standard deviations from the mean centered at the distribution. Therefore, we can truncate it as the mask-type at the specific pixel of each frame. Figure 3-6(b) shows a suitable integer valued convolution mask of Gaussian where σ =1. The Gaussian filter outputs a weighted average of the neighborhood of each pixel. It can provide gentler smoothing and preserves edges better than the normal-sized mean filter due to the distinct size between 5x5 and 3x3. On the other hand, by choosing an appropriately size of Gaussian filter determined by the standard deviation, more range of spatial frequencies is still preserved in the image after filtering because its Fourier form is itself a Gaussian. However, over-wide region contained in the filter will result in the

serious blur effect of the image content. Therefore, the 5x5 principal type of Gaussian mask is still adopted in this part.

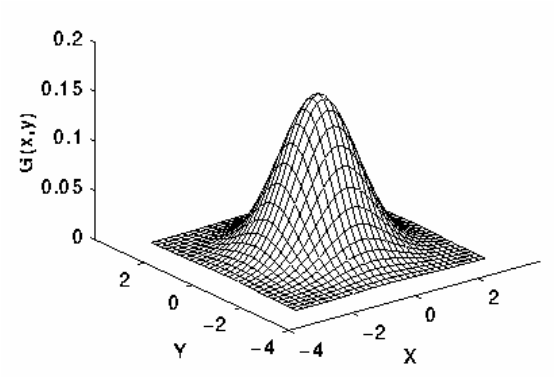

$$\frac{1}{273}$$

1	4	7	4	1
4	16	26	16	4
7	26	41	26	7
4	16	26	16	4
1	4	7	4	1

(a) (b)

Fig. 3-6 : (a) 2-D Gaussian Distribution with mean(0,0) and σ=1. (b) Suitable 5x5 mask of Gaussian filter with σ=1.

Some results of edge detection which describes the details in the next section is preprocessed by Gaussian and Mean filter as shown in Fig. 3-7. Compared with (c) and (d), the extracting method of the lane boundary will be easily disturbed by the remaining noise if the smoothing filter can not effectively remove the high-frequency perturbation.

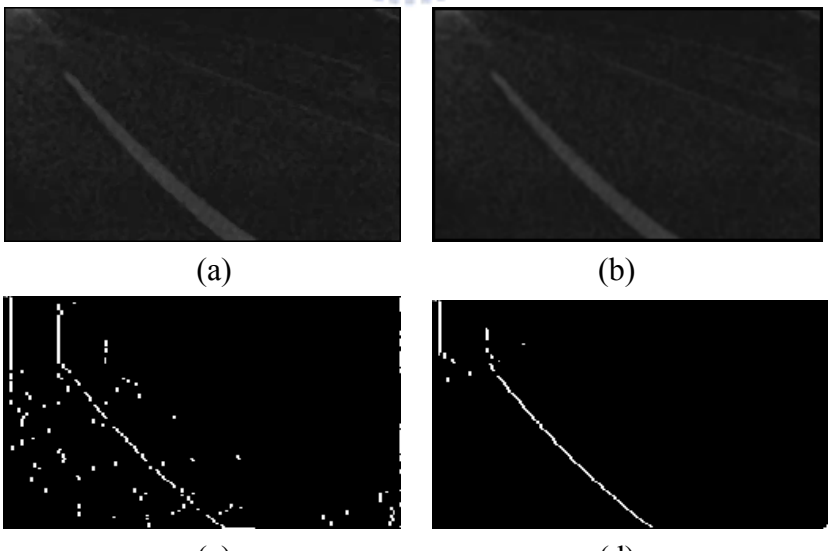

(a) (b)

(c) (d)

Fig. 3-7 : (a) Mean filter. (b) Gaussian filter. (c) Edge detection after (a). (d) Edge detection after (b).

Salt and pepper noise which exist in spatial and time domain is more challenging

for the preprocessing tasks, especially the night environment. To achieve the objective that the effect of the proposed lane detection method in this thesis must be independent on the variation of external light conditions, the time-averaging process focused on the current and previous frames will be added behind the Gaussian smoothing work. The integrated de-noising procedure is demonstrated in Fig. 3-8.

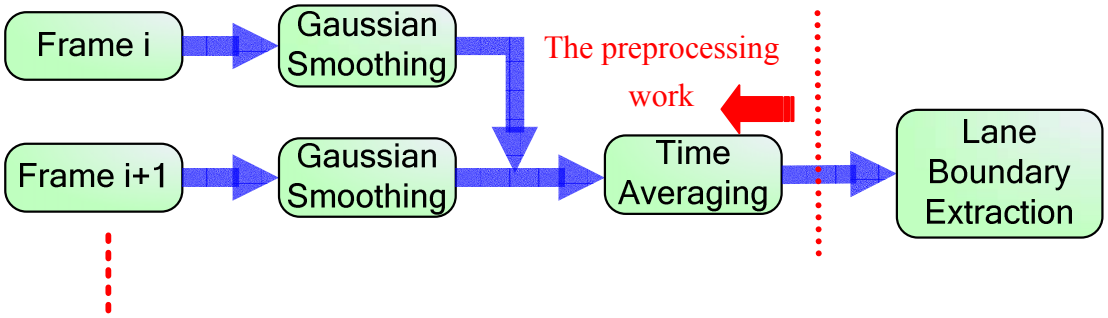

Fig. 3-8 : Flow chart of the complete preprocessing steps.

3.3 Lane Boundary Detection

3.3.1 Edge Detection

The objective in this section is to find the features of lane marker from the information of image. Through the observation, lanes must have some apparent properties about its boundary. The most obvious reason of them is that the lane markers must be brighter than the neighborhood road surface even if they are with various color information. Then, the lane shapes in the image are almost presented as slender types. In other words, extracting the lane boundary is an important step to locate the realistic lane position throughout the video by the foregoing two factors.

The determination of edge detection operators need to be considered the suitable and effective performance for the image contents. Y. Wang [7] and [10] select Canny operator to locate the position of pixels where the significant edge information of

lanes exists by considering the gradient characteristics at the same time. However, using this operator will accompany the obvious computing load since the judging mechanism about the orientation and magnitude of each candidate edge in the whole frame. On the other hand, Kreucher [20] provides a frequency-based extracting method to find the diagonal dominant edges through the partly DCT coefficients. This special concept is so intuitive that the components of edges determined by DCT may be not related to the local information more closely than the common gradient operators, especially about the contents of video acquired by the camera on the side of the vehicle without fixed edge direction of lane markers. By giving the consideration to effects about the systematic performance and the adaptation of video with various view-angles, the LoG (Laplacian of Gaussian) operator is implemented in this step.

LoG is an associative convolution operation which convolves the Gaussian smoothing filter with Laplacian filter of all, and then convolve this hybrid type with the image to achieve the required result for edge detection. As an approximated second-order derivative, the Laplacian mask can highlight the regions where the intensity of pixels contained by the boundary of objects changes rapidly. Nevertheless, this operator can not be used for edge extraction thanks to the higher sensitivity of noise. To reduce this effect, the image has often smoothed by Gaussian before applying the Laplacian mask. Because the second derivative is a linear operation, the hybrid mask of two filters is similar to convolve the Gaussian function first and compute the Laplacian of the result. The 2-D LoG function is shown as follows:

$$
\begin{aligned}
f(x,y) &= -\exp\left(-\frac{x^2+y^2}{2\sigma^2}\right) \\
LoG(x,y) &= \nabla^2 f(x,y) = \frac{\partial^2 f}{\partial x^2} + \frac{\partial^2 f}{\partial y^2} \\
&= -\left[\frac{(x^2+y^2)-\sigma^2}{\sigma^4}\right] \cdot \exp\left(-\frac{x^2+y^2}{2\sigma^2}\right)
\end{aligned}
\tag{3.7}
$$

0	0	-1	0	0
0	-1	-2	-1	0
-1	-2	16	-2	-1
0	-1	-2	-1	0
0	0	-1	0	0

(a)

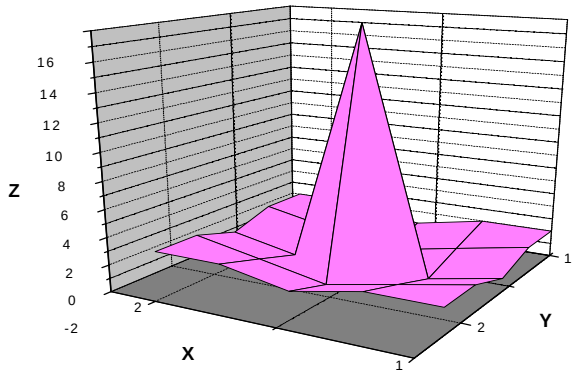

(b)

Fig. 3-9 : (a) 5x5 mask approximation of LoG. (b) 3-D plot of (a).

The 5x5 mask approximation to the LoG function and its 3-D plot is shown in Fig. 3-9. By further observing the property of blind-spot view image from the camera alongside the rear-view mirror, the included angle from the edge of lane to the vertical Y-axis of the image plane must be within the range of degree from 0° to 90°. Compared with other gradient operators, LoG mask has no orientation so that it can not adapt to some specific edge directions of the object. So the additional 5x5 mask similar to the form of the sobel-mask with tilt angle of 45 degree is provided to be combined with the previous LoG mask to adapt to the lateral-view image environment. The convolving relation is explained in the following:

$$I(x,y) * f(x,y) + I(x,y) * g(x,y) \Leftrightarrow I(u,v)F(u,v) + I(u,v)G(u,v)$$

$$I(x,y) * [f(x,y) + g(x,y)] \Leftrightarrow I(u,v)[F(u,v) + G(u,v)] \qquad (3.8)$$

where $f(x,y)$: the LoG mask, $g(x,y)$: the additional 5x5 combining mask

The 3D-plot of new combined mask $f(x,y)+g(x,y)$ will be shown in Fig. 3-10(b). Compared with Fig. 3-9(b), this distribution not only maintains most part of the LoG shape, but also be added the identity of orientation for the blind-spot view due to the “slant” shape in Fig.3-10(b). The results of edge extraction for lane

boundary between the LoG and the new combined mask are demonstrated in Fig. 3-11. According to the result from Fig. 3-11(d), only the intra-boundary of the lane can be extracted, and this property will contribute to link the lane trajectory described in the later section.

0	-1	-2	-3	-4
1	0	-1	-2	-3
2	1	0	-1	-2
3	2	1	0	-1
4	3	2	1	0

(a)

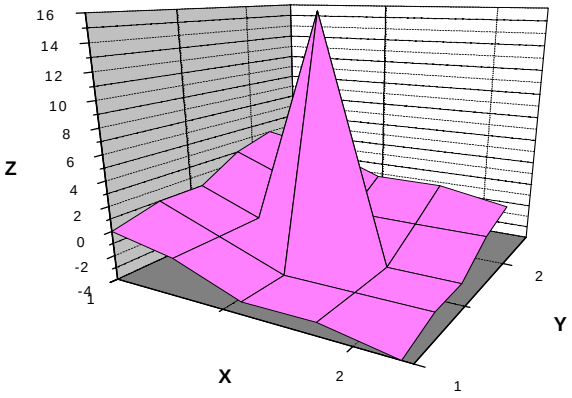

(b)

Fig. 3-10 : (a) The additional mask for LoG combination. (b) 3-D plot of the new 5x5 combined mask.

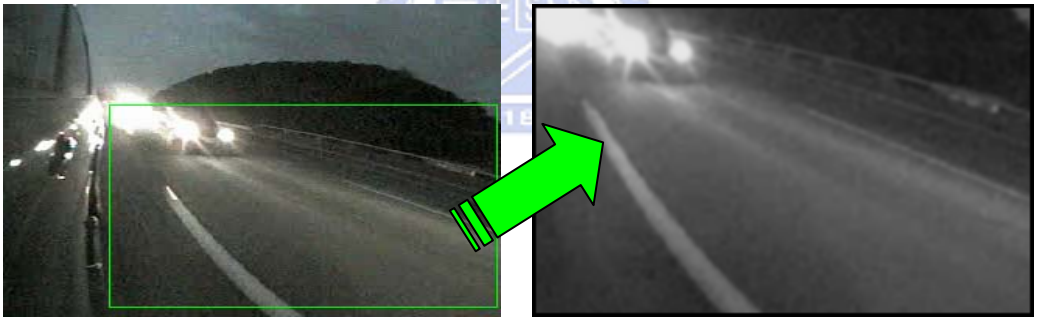

(a) (b)

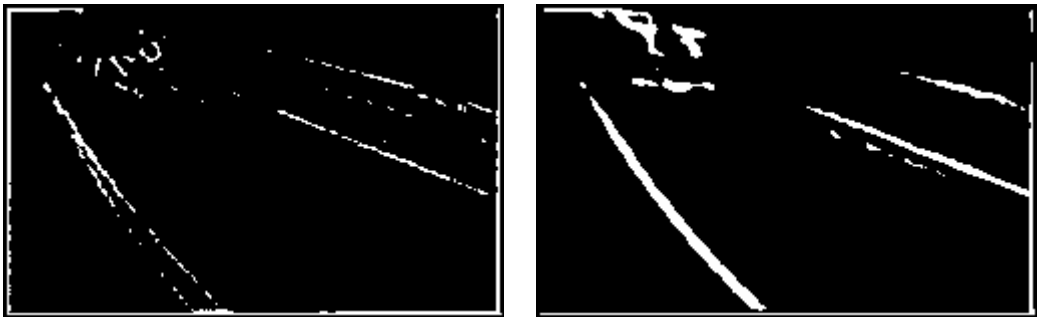

(c) (d)

Fig. 3-11 : (a) The original image. (b) Gaussian smoothing within the ROI of (a). (c) Result of LoG mask. (d) Result of the new combined mask.

The morphological post-procedure is to thin out the lane-marking after the edge

extraction. There are two conditions determining which the pixel can be retained in the image:

if I(k)=255 AND I(k+1)=255
⇒ I(k+N)=0 where N is a little larger than 2
else if I(k)=255 AND k>P(i)
⇒ I(k)=0 where P(i) is the point corresponed to the lane boundary of the row
else
⇒ I(k)=255

The edge-finding approach to determine the location of P(i) will be introduced in Section 3.4.

3.3.2 Adaptive Threshold Determination by Distinct Spatial Region

The pixels within the ROI can be extracted for the image processing tasks in our system. According to the perspective geometry, the length or width of the lane markers within ROI is not the same with each different position. In other words, the lane boundary in the bottom part of ROI is always wider and longer than that in the up part. By considering the transformation effect, the adaptive mechanism is developed to adjust the threshold for different sub-regions, and the size of them depends on ROI.

After processed by edge extraction, the image needs to be decided the threshold for more obvious detecting result. Due to the evidently contrast between the lane markers and the neighborhood road surface, the gradient magnitude of lane boundary caused by the edge operator is usually larger than other locations. Therefore, in this section the values of mean and standard deviation computed by each row within the ROI will be selected as the threshold for different region.

Take the normal distribution for example, the range which contained the distance

for one standard deviation from the mean will account for about 68% of the whole set. Besides, the range will account for about 95% if it contains the distance for two standard deviations from the mean. For each row within ROI in the image, the threshold value is still selected by referencing above scattered property since the gradient magnitude of lane markers is certainly higher than that of the normal road surface. That is,

$$Threshold(j) = \underset{i\in(0,\ \text{width of ROI})}{\text{Mean}} |f(i,j)| + k \cdot \underset{i\in(0,\ \text{width of ROI})}{\text{Standard deviation}} |f(i,j)| \quad (3.9)$$

where k=2,

j : j-th row of ROI,

$f(i,j)$: the value of each pixel within ROI after the edge detection.

The performance of the binarizing approach may be dependent on the edge information of the adjacent moving vehicles close to the lane or the car-light of them, especially the upper part of ROI which can not contain adequate component of the magnitude of lane. Hence, the ROI will be divided into seven sub-regions when it is automatically extracted in the first frame of video, as illustrated in Fig. 3-12

Fig. 3-12 : The division of ROI into seven sub-regions.

Where size= $\frac{\text{height of ROI}}{\text{N-1}}$, N: number of segments (we choose 7 in this system)

In this way, the values of thresholds situated in different location are selected by tuning the mean value of each-row pixels and the arrangement of magnitude for them

are from the bottom to the top sub-region, as described in the following:

$$Threshold(j)=\left(\underset{i\in(0,\ \text{width of ROI})}{\text{Mean}}\left|f(i,j)\right|-\alpha\right)+k\cdot\underset{i\in(0,\ \text{width of ROI})}{\text{Standard deviation}}\left|f(i,j)\right| \quad (3.10)$$

where $\alpha=0.1\cdot\sum_{k=0}^{n}\left(\underset{i\in(0,\ \text{width of ROI})}{\text{Standard deviation}}\left|f(i,j)\right|\right)\cdot k,$

n : n-th sub-region of ROI.

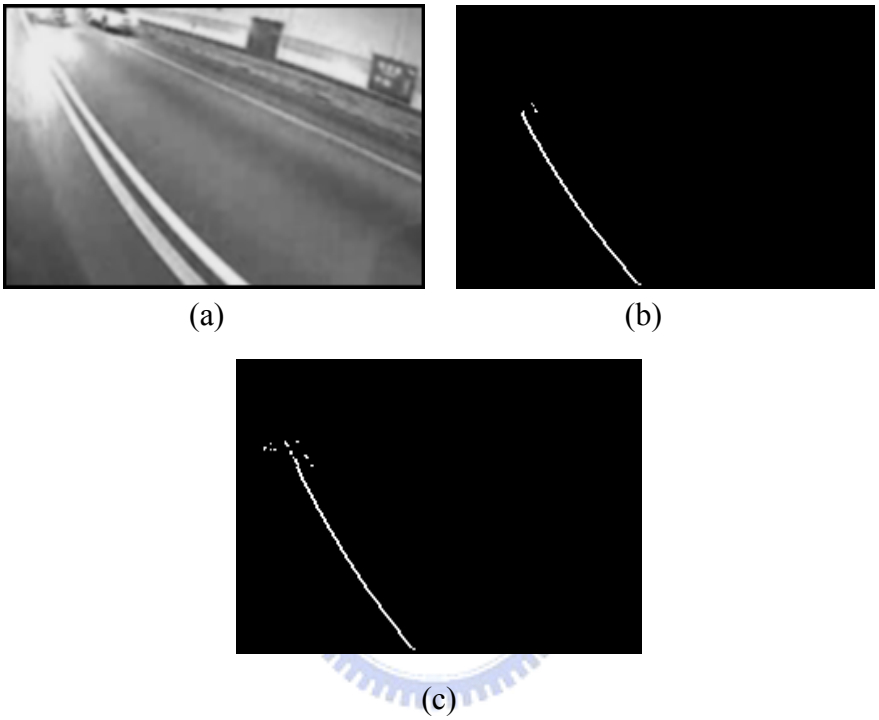

(a) (b)

(c)

Fig. 3-13 : (a) The image is photographed in a tunnel. (b) Lane-marker extraction without considering the sub-region threshold. (c) Lane-marker extraction with considering the sub-region threshold.

Figure 3-13(a) shows an imaging environment about driving in a tunnel. The original lane boundary in the upper region is not easily seen due to the disturbance of the car-light from the backward vehicle, as shown in Fig. 3-13(b). This overexposure effect will be improved by considering the tuning parameter (α) in Fig. 3-13(c).

3.4 Lane-Finding Algorithm

Since the edge information of lane markers has been acquired by the foregoing demonstration, marking and tracking the lane trajectory within ROI can be succeed by such pixels lying on the sides of lane boundary in the image. There have been some researches for lane-model construction. Y. U. Yim and S. Y. Oh [21] use the starting position, direction, and saturation of the lanes regarded as the three features to initialize the lane vector and find the most probable lane trajectory by Hough Transform. Roland Chapuis [25] uses the statistical model to specify the detection ROI in order to narrow the searching area of lane markings. Different from the method merely about the image processing, the lane geometry is taken into the fitting of the lane model provided by A. Lopez [28]. D. J. Kang [30] combines the vanishing point of the road from the frontal camera with Hough Transform for lane tracking.

Based on the objectives for real-time tracking and low-cost computation, a piece-wise edge linking model we proposed in this chapter is effective for lane-shape marking whether the lens-distortion of camera is serious or not.

3.4.1 Distortion Effect of Fish-Eye Camera

A fish-eye lens with a wide angle that takes the extremely wide field of view can cause the hemispherical effect of the image. All the ultra-wide angle lenses of the fish-eye cameras suffer from some amount of distortion. In order to contain the blind-spot region on the side of the car as much as possible, we choose a fish-eye camera as a sensing device for image acquisition.

The distortion effect of lane boundary resulted from the fish-eye camera is shown in Fig. 3-14, which displays the different curvature of lane-shape whether the distance between the lane and the vehicle is so closed or not. Tsai [33] and Hartley [34] provide the algorithms for fish-eye calibration by the internal or external parameters of the camera. However, this kind of information can not be known in advance in our systematic architecture. In other words, the lane-trajectory finding algorithm in this thesis needs to overcome the inherent problem without considering additional computing load for calibration.

Fig. 3-14 : The different curvature of lane in (a) the lane boundary is close to the car-body. (b) The lane boundary is far to the car-body.

3.4.2 Hough Transform

The classical type of Hough transform is to identify the edge or boundary of lines in the image. This principle is to transform the X-Y coordinate system into the r-θ parameter space, where r represents the small distance between the line and the origin of the image, and θ is the angle of the locus vector from the origin to this closest point. The relationship of the transformation about two coordinate systems is shown in Fig. 3-15. According to equation (3.11) from this figure, they can determine if the point A and B are colinear with the same r and θ. Besides, equation (3-12) is to determine if the line segment formed by A and B is collinear with that formed by C

and D by judging the condition that the parameter d is smaller than a threshold.

$$r = x_1 \cdot \cos\theta + y_1 \cdot \sin\theta = x_2 \cdot \cos\theta + y_2 \cdot \sin\theta \tag{3-11}$$

$$d = \left| r - (x \cdot \cos\theta + y \cdot \sin\theta) \right| \tag{3-12}$$

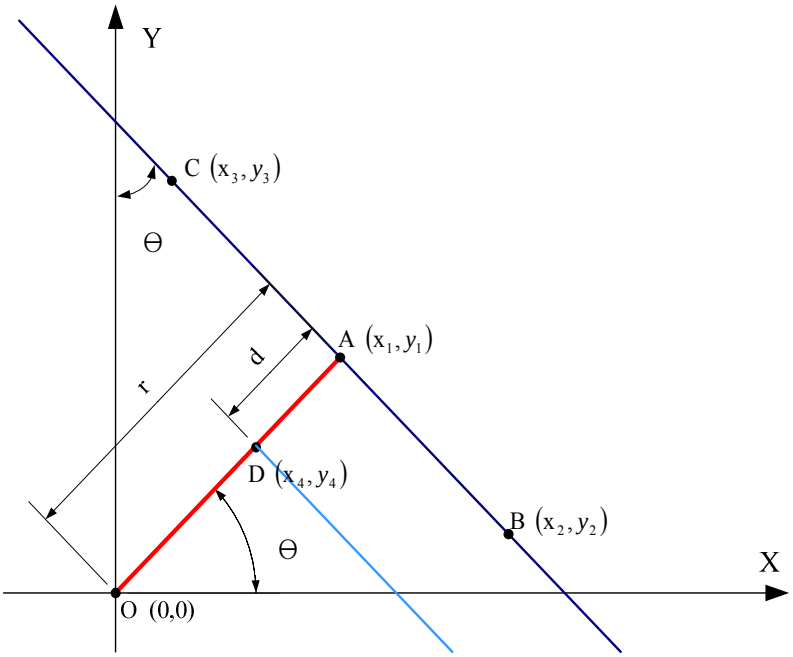

Fig. 3-15 : The diagram of relationship between the x-y and r-θ coordinate systems.

3.4.3 Piece-Wise Edge Linking Model

Qing Li [22] and C. H. Yeh [24] still apply the Hough transform to track the lane markers which can not be deformed in the image captured by the normal camera. However, due to the distinct curvature with the fish-eye lens, it is impossible to take Hough transform into our system. Hence, the novel approach for lane modeling needs to be considered the geometric effect of ROI and the connectivity of the lane markers with robustness and adaptation.

The flow chart of the piece-wise edge linking model is shown in Fig. 3-16(b).

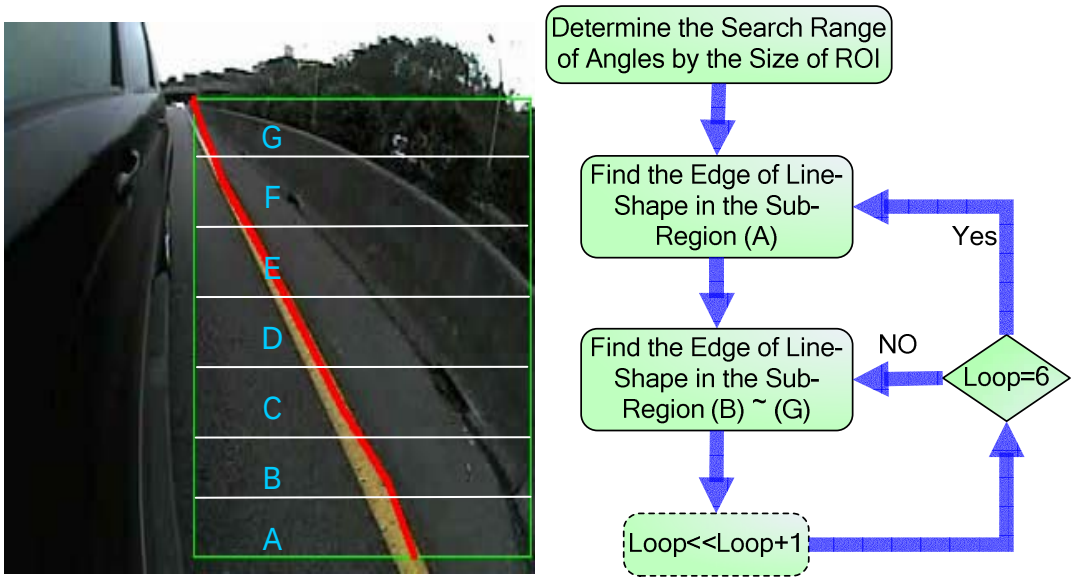

(a) (b)

Fig. 3-16 : (a) Seven sub-regions automatically segmented within ROI. (b) The flow chart of the piece-wise edge linking model.

(a) (b)

Fig. 3-17 : (a) Seven sub-regions segmented within ROI. (b) The flow chart of the piece-wise edge linking model.

Figure 3-17 shows the two different size of ROI is caused by the variation of the intrinsic and extrinsic setting of camera. In general, the width of ROI depends on the yaw angle of camera, and the height of that depends on the pitch angle or the distance from the mounting position near the rearview mirror to the road plane. Although those parameters can not be taken in our system, we still find the property that the lane boundary in the image must extend to the upper-left part of ROI even if the lateral position estimated from the lane marker is not the same through the image sequences.

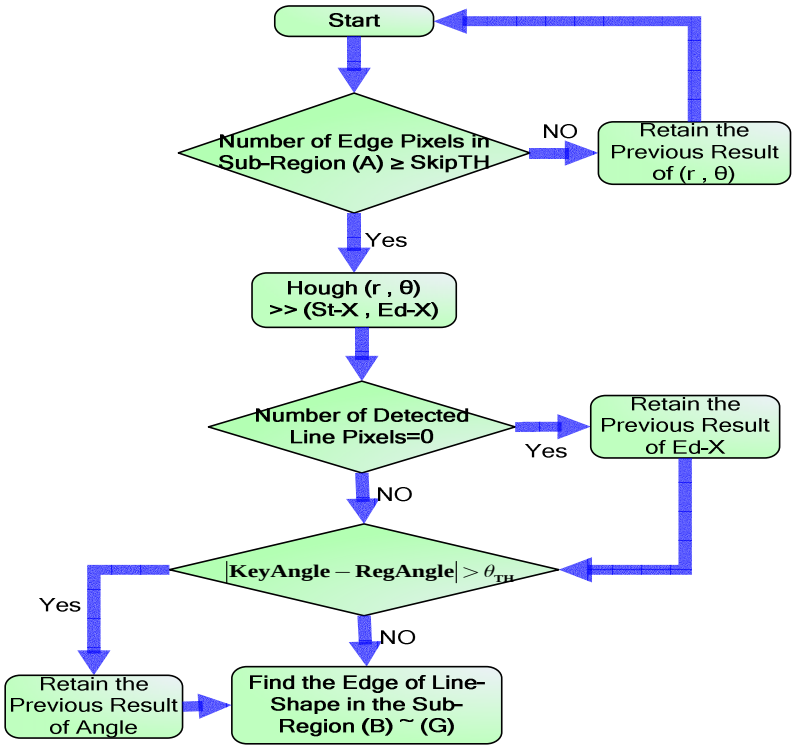

Fig. 3-18 : The flow chart for finding the line-shape in the bottom sub-region (A).

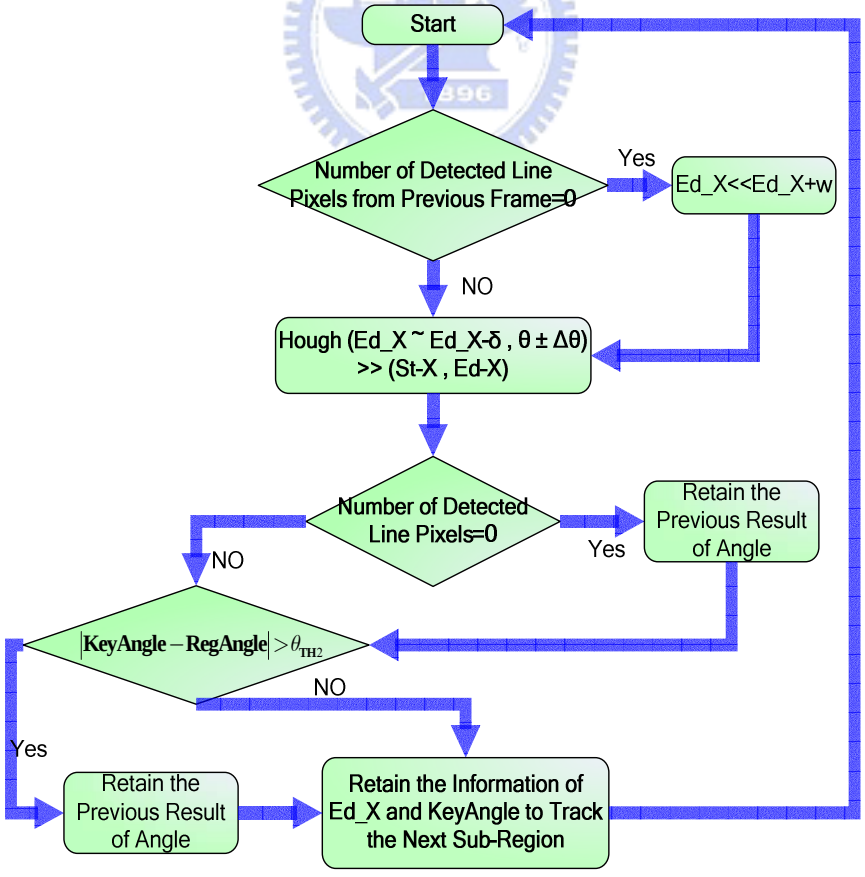

Fig. 3-19 : The flow chart for finding the line-shape in sub-regions from (B) to (G).

By using the perspective effect that lane markers almost converge near the region of vanishing point, the included angle from the diagonal of the ROI to the vertical boundary of that can be determined the maximum searching range of angles for Hough transform. This mechanism will be regarded as the initial step in the piece-wise linking model as shown in Fig. 3-16(b). To overcome the irregular curvature of lane trajectory from the fish-eye lens distortion, the seven sub-regions automatically segmented in Fig. 3-16(a) contribute to fit the edge pixels of lane since its boundary information contained in it can be regarded as the line-shape. Therefore, the principle of Hough transform described in Section 3.4.2 is directly used for the bottom sub-region (A) as demonstrated in Fig. 3-17. The details of parameters in Fig. 3-18 and Fig.3-19 are explained as follows:

St_X, Ed_X:

The coordinate values of x-axis in the bottom and top border of the sub-region determined by Hough transform. Ed_X situated in the bottom border of the next sub-region, such as the same location as the bottom border of sub-region (B) and the top border of sub-region (A), can become the fixed point for searching the line edge pixels only by the angle θ as the flow chart in Fig. 3-19.

SkipTh:

Its size depends on the vertical pixel-width of the sub-region (A) in Fig. 3-18. For some circumstances like the rapidly lane changing maneuver, the lane marker may be discontinuous for each sub-region in the image. The threshold is to control when the lane modeling procedure is performed and observe if the edge pixels in the bottom sub-region (A) have adequate amounts to composite the lane trajectory.

KeyAngle, RegAngle, θ_{TH} , θ_{TH2} , δ, Δθ, Lw:

KeyAngle and RegAngle are the angles about appropriate orientation of line boundary in sub-regions induced by the current and previous frame. Based on the connectivity and continuity of lane markers on the road surface, θ_{TH} and θ_{TH2} are the thresholds to limit if the difference between KeyAngle and RegAngle is small enough. In addition, θ_{TH2} must be smaller than θ_{TH} since the searching angles with sub-region (B) to (G) is restricted by the previous detecting results from the bottom sub-region (A). δ and Δθ are the slight range for detection with Hough Transform from sub-region (B) to (G) where the computation power can be reduced. At last, Lw is a revised parameter to restart the seeking area in the x-axis when the number of line pixels is zero in Fig. 3-19.

To simply the geometric circumstance that the distance between the vehicle and lane trajectory with some curvature in the image is much different, especially the effect of fish-eye lens distortion, we use LSR (least square regression) to make the curved a lane boundary approximate a straight line. The LSR can be induced as below:

$$\boldsymbol{E}=\sum_{i=1}^{n}\boldsymbol{e}_i^2=\sum_{i=1}^{n}(\boldsymbol{Y}_i-\boldsymbol{a}\cdot\boldsymbol{X}_i-\boldsymbol{b})^2 \tag{3-13}$$

$$\begin{cases}\dfrac{\partial \boldsymbol{E}}{\partial \boldsymbol{a}}=\sum_{i=1}^{n}2\cdot(\boldsymbol{Y}_i-\boldsymbol{a}\cdot\boldsymbol{X}_i-\boldsymbol{b})\cdot(-\boldsymbol{X}_i)=0\\ \dfrac{\partial \boldsymbol{E}}{\partial \boldsymbol{b}}=\sum_{i=1}^{n}2\cdot(\boldsymbol{Y}_i-\boldsymbol{a}\cdot\boldsymbol{X}_i-\boldsymbol{b})\cdot(-1)=0\end{cases} \tag{3-14}$$

Equation (3-13), (3-14) can be simplified as

$$\begin{cases}\boldsymbol{a}\sum \boldsymbol{X}_i^{\,2}+\boldsymbol{b}\sum \boldsymbol{X}_i=\sum \boldsymbol{X}_i\boldsymbol{Y}_i\\ \boldsymbol{a}\sum \boldsymbol{X}_i+\boldsymbol{b}\cdot\boldsymbol{N}=\sum \boldsymbol{Y}_i\end{cases} \tag{3-15}$$

$$\begin{cases} a = \dfrac{\begin{vmatrix} \sum X_i Y_i & \sum X_i \\ \sum Y_i & N \end{vmatrix}}{\begin{vmatrix} \sum X_i^{\,2} & \sum X_i \\ \sum X_i & N \end{vmatrix}} \\ b = \dfrac{\begin{vmatrix} \sum X_i^{\,2} & \sum X_i Y_i \\ \sum X_i & \sum Y_i \end{vmatrix}}{\begin{vmatrix} \sum X_i^{\,2} & \sum X_i \\ \sum X_i & N \end{vmatrix}} \end{cases} \tag{3-16}$$

Where N= (Numbers of sub-regions in ROI) + 1

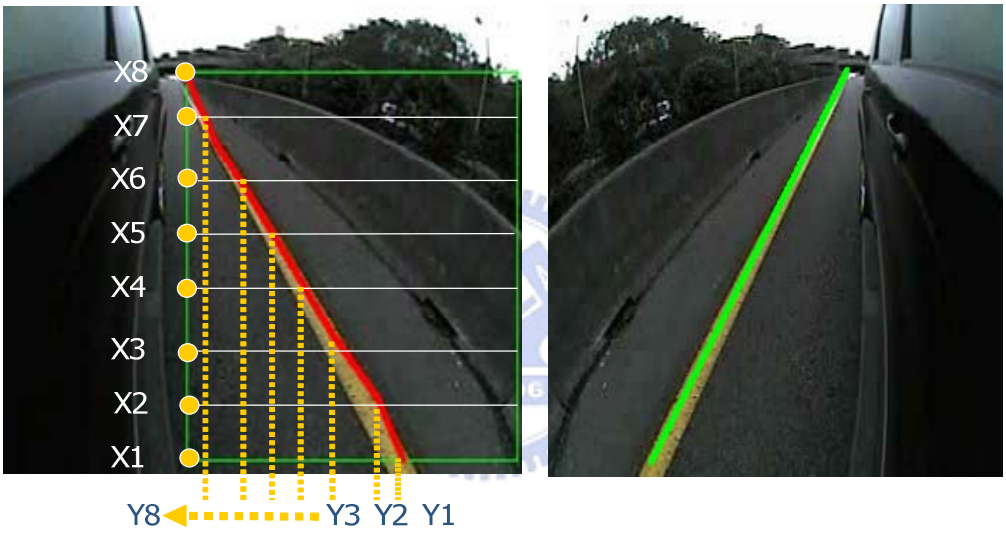

Fig. 3-20 : LSR approximation.

According to the parameter information showed in Fig. 3-20 (a), the linear model can be constructed by the equations (3-16). The approximating straight lane boundary is displayed in Fig. 3-20 (b), which is directly reflected since the image contents acquired by the camera mounted on the opposite side of the vehicle are almost the same except for the reflective property.

Chapter 4

Lane Departure Warning and Drowsiness Estimation

4.1 Overview

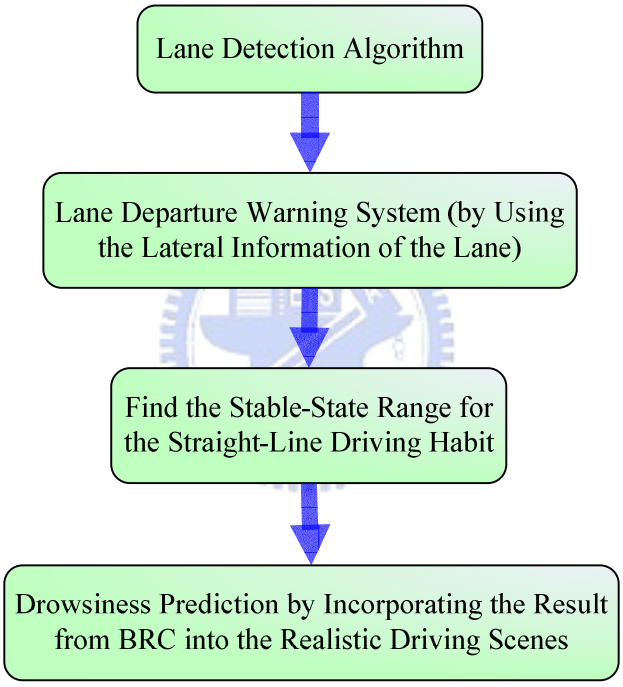

Fig. 4-1 : The flow chart for the whole system.

After extracting the lane boundary from the previous chapter, the lateral information of lane markers can be used to judge when the lane change maneuver occurs for the driver. In this chapter, the LDW (lane departure warning) system is constructed by measuring the displacement, instantaneous velocity and TLC (time to lane crossing) of the lane to form the warning triggers for alarms. The standard for drivers' drowsy state is based on the reflection time when people start to turn the

steering wheel after they drive off the stable-state regions which are dependent on the habit of them for strait-line driving. Trying to combine the experimental data from BRC (brain research center) in NCTU with the realistic scenes, and a gauge of drowsy degree will be proposed to show the possibility with respect to the drowsiness of drivers. The flow chart of the whole system is shown in Fig. 4-1.

4.2 Lane Departure Warning

4.2.1 The Warning Algorithm

As described in Section 1.2.2, some algorithm has been developed to predict when the driver is in danger of departing the road but not annoy the driver sensitively. In other words, extending the interval of warning time can receive the more correct driving maneuver, but the number of nuisance alarms will increase apparently. Lee [26] and Ruder [31] considered that LDW does not necessarily need the precise offset and position information from each frame to add the computing load since it only assists the human driver and passively responds to the circumstance such as when the lane-departure occurs. In order to balance the systematic efficiency and acceptable detection rate in our LDW system, only two representative measures are selected to trigger the warning message. The two judging conditions are discussed as follows:

(1) Lateral displacement:

If the lane boundary is excessively close to the vertical borders of ROI, the driver will be in danger with higher possibility. We will regard this as a dangerous departing behavior even if it may be only someone's habit of driving. There, the safe region which contains the normal lateral offset of lanes is defined as follows.

$$\text{Safe Region: } \left\{\frac{1}{4}\mathbf{ROI}, \frac{4}{5}\mathbf{ROI}\right\}$$

(2) TLC (time to lane crossing):

TLC which was first proposed by Godthelp [35], is a measure of the time remaining before a vehicle on a given trajectory will depart the road. It can provide more reliable information than the lateral position merely due to the factor for lateral velocity can be considered. In our system, the definition of TLC is a ratio of lateral offset smaller than the width of ROI to the lateral velocity at the moment.

The classification for the dangerous degree of warning alarms and the deducing process of TLC are explained in details in the next section.

4.2.2 Evaluation

To prevent the noisy effect such as high frequency variances of the lateral offset of lane markers in each frame from measuring error, we take five frames processed by lane detection to estimate only one weighted average result for departure judgment such like a causal temporal filter. (In practice, there is always one frame only for Gaussian smoothing between the two frames used for lane detection in our system. In other words, consecutive five numbers of lateral positions occupy about 0.33 seconds for 30fps.) The values of weights are {0.22, 0.21, 0.20, 0.19, 0.18} from the present and the last four processed frames. The flow chart for TLC computation is shown in Fig. 4-2.

By the two obvious measures, the degree of departure warning can be classified with the color of alarms as the following:

If the current lateral offset is inside the safe region: $\{\frac{1}{4}\text{ROI}, \frac{4}{5}\text{ROI}\}$

If $\text{TLC} \geq 2.5\text{sec}$ AND $\text{Vel} \neq 0$

Alarm type >> green light

Else

Alarm type >> yellow light

Else

Alarm type >> red light

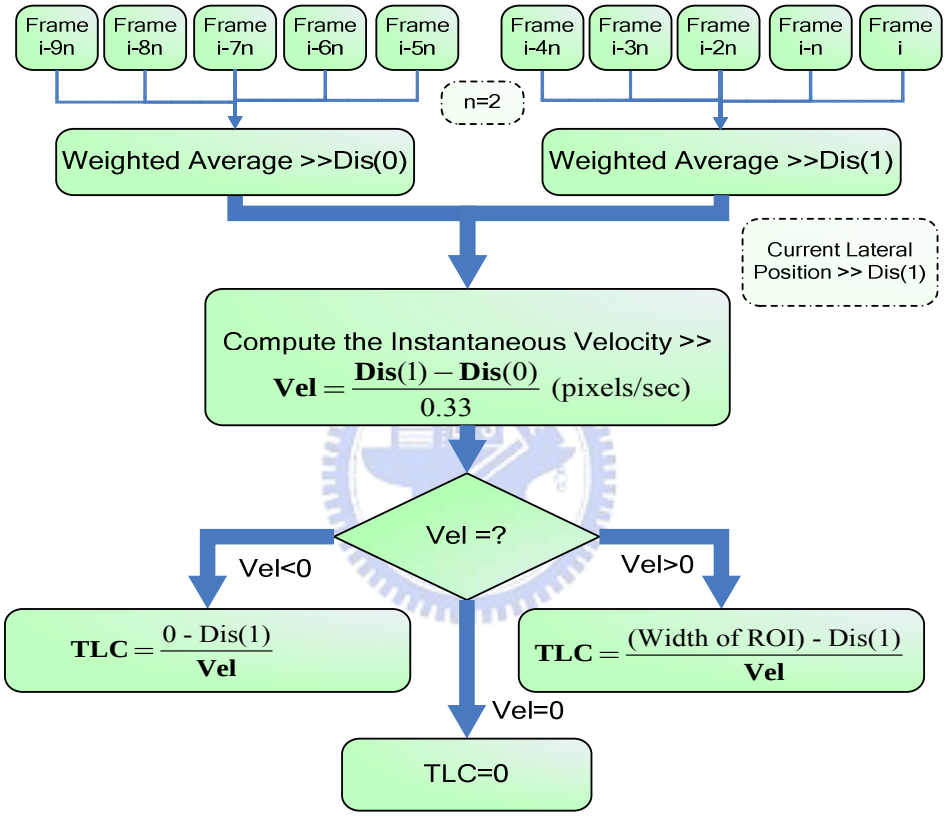

Fig. 4-2 : The flow chart for TLC estimation.

4.3 Drowsiness Estimation for Driver

In recent years, preventing accidents caused by drowsiness has become a major focus of active safety driving in recent years. The major challenges in developing a real-time system for drowsiness prediction include: 1) the lack of significant index for detecting drowsiness and 2) complicated and pervasive noise interferences in a

realistic driving environment. Therefore, the BRC (Brain Research Center) in National Chiao Tung University has developed a drowsiness-estimation system based on electroencephalogram (EEG) to estimate a driver's cognitive state when he/she drives in a virtual reality (VR)-based dynamic simulator. The definition of the driving error in this experimental environment is the deviations between the center of the vehicle and the center of the cruising lane in the lane-keeping driving task.

In this section, the system architecture of BRC will be introduced in Section 4.3.1. The relationship between the reaction time and driver's drowsiness will be explained in Section 4.3.2. Before trying to reasonably and effectively integrate the measuring result from the VR-based driving environment into the lane detection system in this thesis, some changeful factors of the realistic image-based system must be discussed. In Section 4.3.3, a stable-state range can be constructed to determine the lane's lateral position where someone gets used to driving in a straight road-path for a long time. Then, a gauge of the drowsy degree successfully combine the experimental result evaluated by the EEG-based analysis [27] with the realistic and dynamic LDW system successfully is proposed in this thesis, as described in Section 4.3.4. Finally, in order to adaptively extend the experimental framework to the practical driving environment, we estimate the average velocity within the interval of reaction time by deducing the ratio of the lane-width on the realistic road plane to that in the video, as explained in Section 4.3.5.

4.3.1 Experimental Architecture of BRC

In general, measuring the precise data for human consciousness in dynamic driving environment is not easy. There may be some perturbations from the external noise or suddenly interference caused by the traffic variations affecting the data

accuracy. In other words, strict training of human operators by the actual machines or vehicles in real sites not only has high demands in space, time, and money to perform such a training job, but also leads to another phase of the measuring problem. To overcome the above dilemma, the worldwide trend is to use the virtual-reality (VR) technology to meet the requirements of public security in training and censoring of human operators. It can provide a realistic safety environment, which allows subjects to make on-line decisions by directly interacting with a virtual object rather than monotonic auditory and visual signals. Besides, VR is also an excellent candidate for brain research on real-time tasks become of its low cost, saving time, less space, and condition control to avoid the risk of operating on the actual machines, and thus extends the applications of possible brain computer interfaces to general populations.

Fig. 4-3 : The VR-based dynamic driving simulation laboratory.

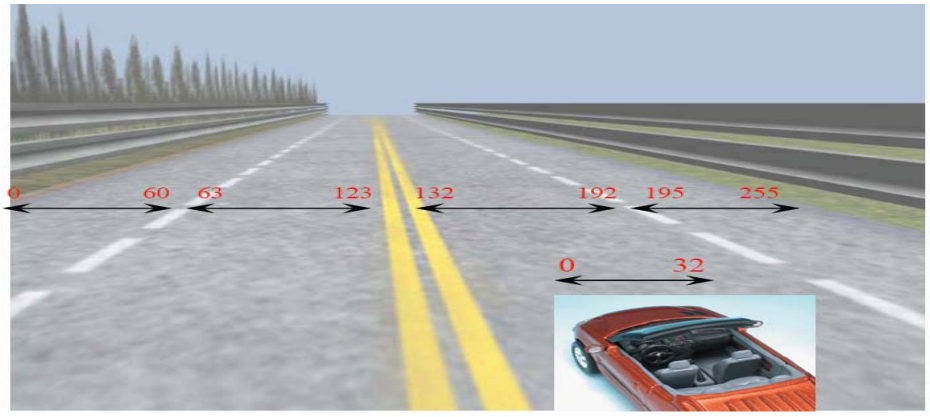

Fig. 4-4 : The details about the width information of each lane, road, and car.

The experimental environment constructed by BRC is shown in Fig. 4.3. The VR-based four lane highway scene is projected on a 120 degree-surround screen (304.1-cm wide and 228.1-cm high), which is 350 cm away from the driving cabin. The four lanes from to right are separated by a median stripe. The distance from the left side to the right side of the road is equally divided into 256 points (digitized into values 0-255), where the width of each lane and the car is 60 and 32 units, respectively. The frame rate of highway scene is 60 fps. All the descriptions are depicted in Fig. 4-4.

4.3.2 Predictive Mechanism for Drowsiness Effect

Before executing the experimental step, we have to find the relationship between the measured EEG signal and the subject's behavior performance. One point should be taken as a quantified index as the deviation between the center of the vehicle and that of the cruising lane [36]. By examining the video recordings, the pilot experimental studies show that when the subject is drowsy, the driving performance will decrease and vice versa. In this experiment, the subjects participated in the highway-driving simulation after lunch in the early afternoon when the alertness may easily diminish within one-hour monotonous working [37].

All the subjects were instructed to keep the car at the center of cruising lane by controlling a steering wheel. In all sessions, the subjects drive the car continuously for 60 minutes and were asked to try their best to stay alert. Participants then returned on different days to complete a second 60-minute driving session or more if necessary. To mimic the consequences of a non-ideal road surface, the car is randomly drifted away from the center of the cruising lane every 5 or 10 minutes. So the driver must maintain high attention to immediately correct the direction of vehicle in the cruising

lane due to the 60 pixels per second for the deviating velocity. When the driver is drowsy, the reaction time between the onset of deviation and steering wheel is increased. This event can be used for ERP analysis of different drowsiness states using 30-channel EEG signals [27].

In general, the reaction behavior should be increasingly slower when people start to enter the drowsy state. In other words, the higher possibility for the measurement shows that the subject is drowsy when his/her average reaction time is gradually longer in a section of time interval. To avoid the fluctuation of drowsiness signal, the measured data for reaction time must be smoothed by a causal 90-second square moving average filter advancing at 2-seconds steps. The experimental trials are sorted according to the length of reaction time and equally divided into five groups as the index for drowsiness estimation in Fig. 4-5, where each group has 20 percentages of trials in order. This statistics evaluated by the EEG analysis [27] can be regarded as the reference implemented into our vision based lane departure warning system.

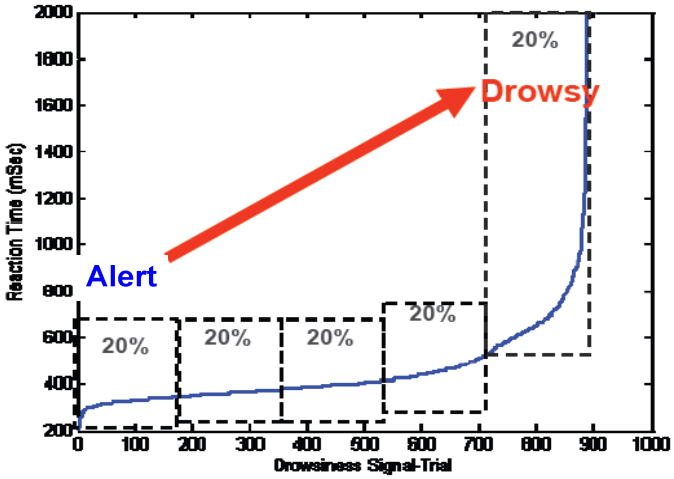

Fig. 4-5 : The trials collected from the VR-based experiment are sorted according to the degree of reaction time.

4.3.3 Construct the Stable-Driving Region with Different Driver's Habit

According to the above experimental condition, the definition of reaction time is the duration between the onset of deviation and the occurrence for steering-wheel. Subjects have to move the vehicle's center back to the cruising lane to wait for the next testing deviation produced by the computer when they have been informed in advance. However, the restarting action is not easy to be determined due to the variation of different driving habits, especially the loose drivers which have a larger spread in lateral position so that the distance between the wheel and lane marker can not exactly fixed in the straight-road driving [15]. Therefore, the algorithm to extract the stable-state driving region must be developed before constructing the drowsiness estimation mechanism.

The standard for stable-state range determination is described as below: (1) the lateral position of lane markers within this region should be close to each other; (2) the TLC is larger; (3) The lateral offsets found by the LDW system in Section 4.2 must be situated in this region for a long period.

According to the above properties, first of all, we take the lateral offsets with larger TLC about consecutive N frames processed by the LDW system. Second, by the previous statistics, the mean and standard deviation estimated by them with the clustering method are used to model the region as a normal distribution. At last, the updating method is developed to adjust the size and location of the range to the changed driving habit for a driver. The flow chart for stable-state region determination is demonstrated in Fig. 4-6.

To rapidly and precisely find out the optimal parameters of each normal

distribution, we choose k-means to initially classify the statistics of N lateral offsets.

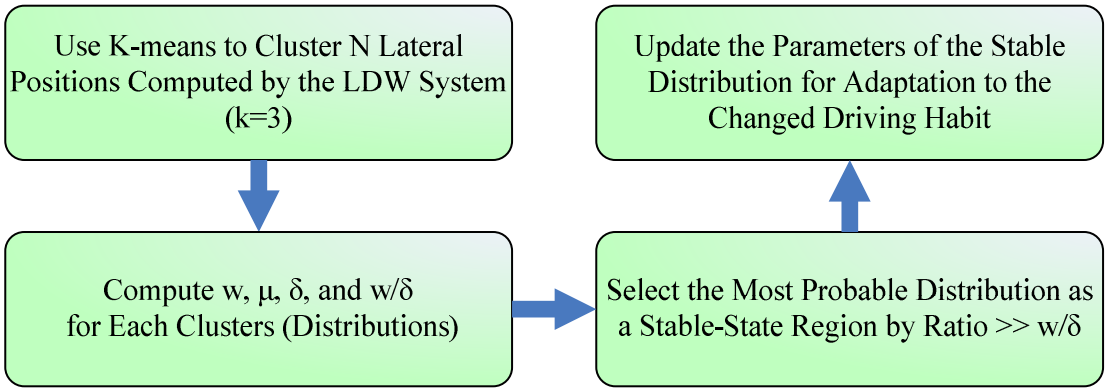

Fig. 4-6 : The flow chart for stable-state region determination.

The error function which determines the clustering center point of each group is shown as follows:

$$d_i = \sum_{i=1}^{k} \sum_{x_j \in P_i} (x_j - \mu_i)^2 \qquad (4\text{-}1)$$

where μ_i is the centroid or mean point of all the points $x_j \in P_i$,

P_i is the i-th of k clusters, $i = 1, 2, ...k$.

In Fig. 4-6, μ is the mean value of each distribution; δ is the standard deviation of each distribution; w is the weight determined by the probability of each group. After initializing for each distribution model, we find that the N lateral offsets can be approximately modeled by only three normal distributions, which are respectively located on the points nearby the mean value and 1.5 standard deviations with high probably, as shown in Fig. 4-7. Therefore, we choose K=3 as the initial clustering numbers.

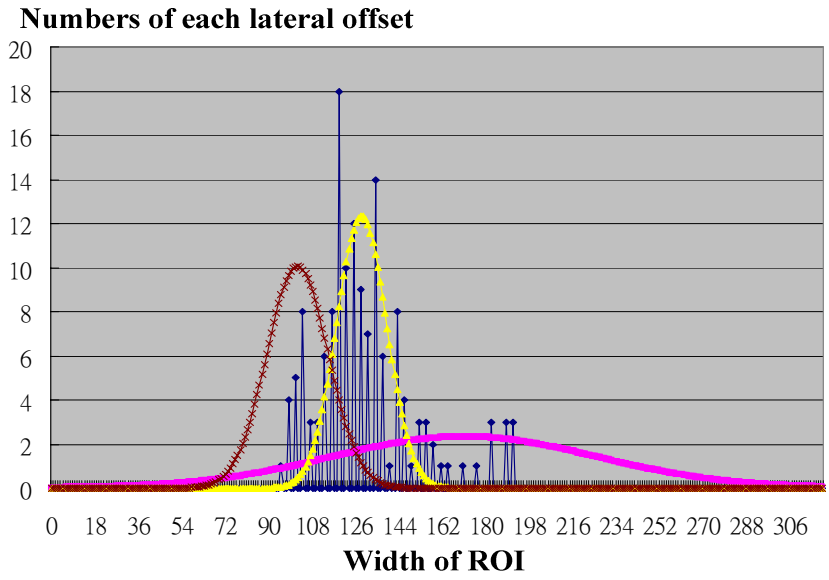

Fig. 4-7 : The distribution of N lateral offsets and three approximately Gaussian model (N=200 in this Figure.)

Not the same as the adaptive background model [32], the human habit can last within a steady behavior style for a long time. Based on this psychological property, we only use a single normal distribution with some update mechanism to model the adaptive stable-state driving region to avoid its unreasonable fluctuation. Updating the parameters of the stable-state model can adapt to the changed driving habit if the lateral offset is within 2.25 standard deviations of this distribution. The parameters of the distribution which matches the new observation for human habit are updated as follows:

$$\mu_t = (1-\beta)\cdot\mu_{t-1} + \beta\cdot x_t \tag{4-2}$$

$$\sigma_t^2 = (1-\beta)\cdot\sigma_{t-1}^2 + \beta\cdot(x_t-\mu_t)^2 \tag{4-3}$$

where $\beta = \alpha\cdot\eta(x_t \mid \mu_k, \sigma_k)$, α is the learning rate

$$\eta(x_t,\mu_t,\sigma_t) = 1/[(2\pi)^{1/2}\cdot\sigma_t]\cdot e^{-\frac{1}{2}(x_t-\mu_t)^2\cdot\sigma^{-1}}. \tag{4-4}$$

By observing equation (4-5), the influence for this stable-driving distribution will be unapparent when the distance between the current lateral offset and the mean value of the model is so far. This property can effectively maintain the stability of this region.

4.3.4 Data Collection and Adjustment for the Realistic Environment

After selecting the suitable driving region for the driver, the experimental statistics evaluated by EEG analysis from BRC can be integrated into our lane departure system. Not the same as experimental condition which stipulated that the reaction behavior can be increasingly slower when the subject starts to enter the drowsy state by observing the trend of reaction time for a long period (about 90 sec), the demand for drowsy estimation mechanism in our system should provide real-time prediction if the driver is still on the alert. Therefore, we design a gauge chart to estimate and display the current driver's drowsy degree as much as possible, as shown in Fig. 4-8 (b).

In Fig. 4-8 (a), the difference in lateral offset between (B) and (C) is 52.45 pixels, the mean value (A) of stable-driving region is located at pixel value of 123.23, and the reaction time counted from (D) and (E) is 1.65sec, as shown in Fig. 4-8 (c).

As described in Section 4.3.2, the definition of reaction time is the time interval of deviation between the center of the vehicle and that of the cruising lane in the VR-based experimental environment. In other words, the value of deviation can be the same as the lateral offset between the car-body and the lane marker in our vision-based system. By the known stable-driving region determined in Section 4.3.3,

the drowsiness estimation system can apply to drivers with different driving habits without directly selecting the unchanged center part of ROI, such as the restarting mechanism of BRC. Therefore, the count of reaction time starts when the lateral offset of lane marker deviates outside the stable region, and stops when the driver turns back the steering wheel exactly in our system. However, since we judge the reactive behavior only by the image contents, the backward motion must be confirmed by the criterion that the direction of the lateral velocity keeps identical until the lateral offset is within the stable region again, as the points (D) and (E) in Fig. 4-8 (d) separately.

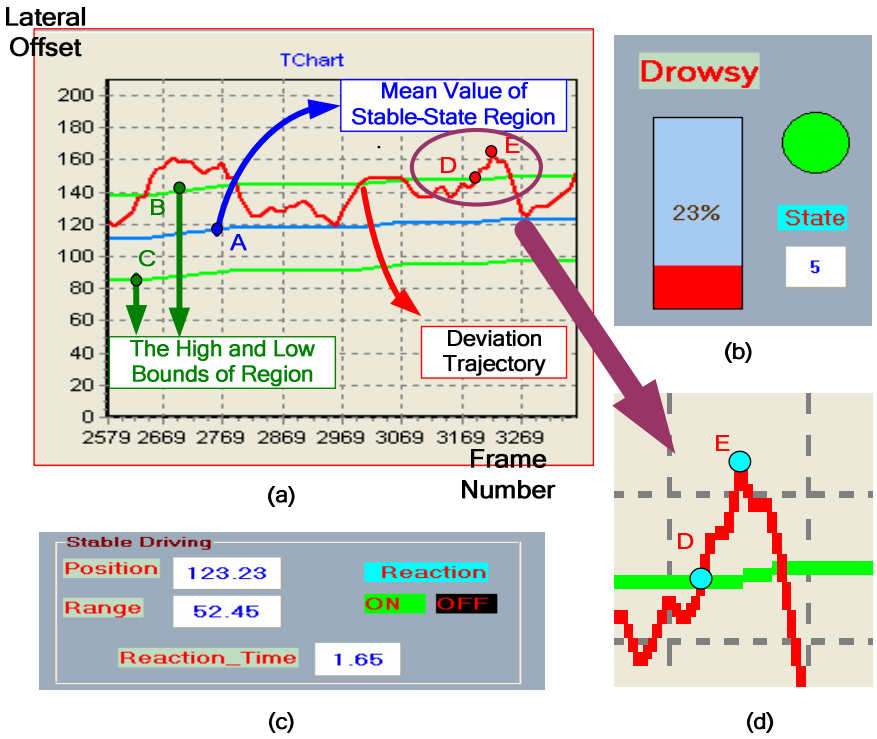

Fig. 4-8 : The mechanism for drowsiness estimation in our LDW system. (a) The relationship between the stable-state region and the lateral deviations. (b) A drowsy-degree gauge chart. (c) A stable-driving group box, (d) The start and stop points of reaction time.

The flow chart for drowsy degree estimation by the reaction time is shown in Fig. 4-9. The discussions about Fig. 4-9 are described as follows:

(1) The drowsy degree may be subtracted by 10% if the reaction time is never up to 1.5sec for 10sec. This automatic mechanism is based on the VR-based experiment of BRC that the computer will automatically produce the deviation behavior about 5~10sec. After all, the reactive behavior in drowsy state must be increasingly slower without reducing the alert abruptly.

(2) The variation of drowsy degree displayed in the gauge chart, as demonstrated in Fig. 4-8 (b), depends on the estimated reaction time of the driver in the realistic environment. To avoid the variances in drowsy degree violating the nature of human operation, the changeful region for each estimation result is limited within plus and minus 20%.

(3) Use the classified alert and drowsy state in Fig. 4-5 analyzed by EEG-based algorithm as the evidence to determine the cognitive property of the driver in realistic environment.

(4) If the drowsy degree is exceeded 70%, the alarm light with red color will be displayed in our system. On the other words, the alarm light with yellow color will be turned on if the drowsy degree is exceeded 35% but not up to 70%. Otherwise, the green light is showed that the driver is still situated in the safety-state with higher alert.

(5) In general, the lane change maneuver can be not certainly judged as an intentional action for driving or an unintentional behavior with the drowsy consciousness only by the information of deviations. Therefore, the warning mechanism focused on this departing behavior is described as below:

If Pos(t)-Pos(t-k)>0.8·(width of ROI)

≫ This departing motion is recognized as the lane change maneuver

If Drowsy Degree ≥ 70% (red light)

Not change

≫ Caused by the drowsy consicousness

Else

Drowsy Degree=0

≫ Caused by the intentional behavior for normal driving

Where

Pos(t): The currently measured lateral offset

Pos(t-k): The previously measured lateral offset, k is dependent on the frame rate of video

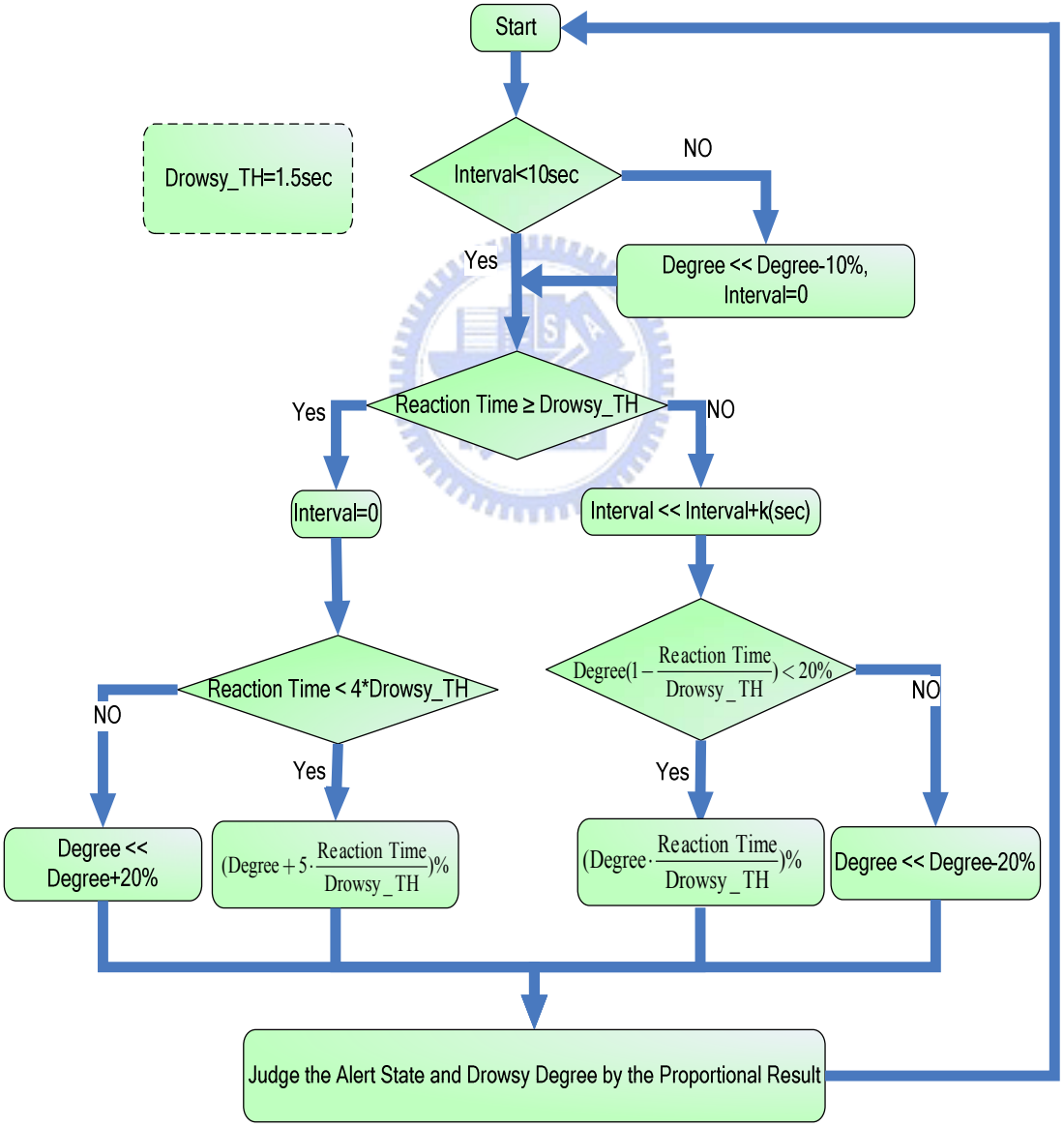

Fig. 4-9 : The flow chart of drowsy degree estimation by the average reaction time evaluated from BRC.

Chapter 5

Experimental Results

5.1 Environmental Setup

Figure 5-1 shows that a fish-eye camera is mounted under the rear-view mirror on the side of the vehicle to acquire blind-spot view image sequences. In addition, the driver can immediately obtain the sideward information of road surface by the CRT which displays the real-time image sequences from the outside camera.

Fig. 5-1 : The experimental architecture.

Table 5 : Specification of platform information.	
CPU	**Intel T5600 1.83GHz**
Memory	**1GB DDR2 RAM**
Compiler	**Borland C++ Builder 6.0**
OS	**Microsoft Windows XP**
Resolution	**320x240**
Frame rate	**30 FPS**

Figure 5-2 shows the realistic programming interface in the PC platform. Block (A) contains the input frame which is added the approximating straight lane boundary by LSR, as explained in Chapter 3, in the left part; the center part of (A) shows the result of lane detection method with ROI extraction; the right part of (A) which shows the binarizing lane boundary only includes the image contents within ROI.

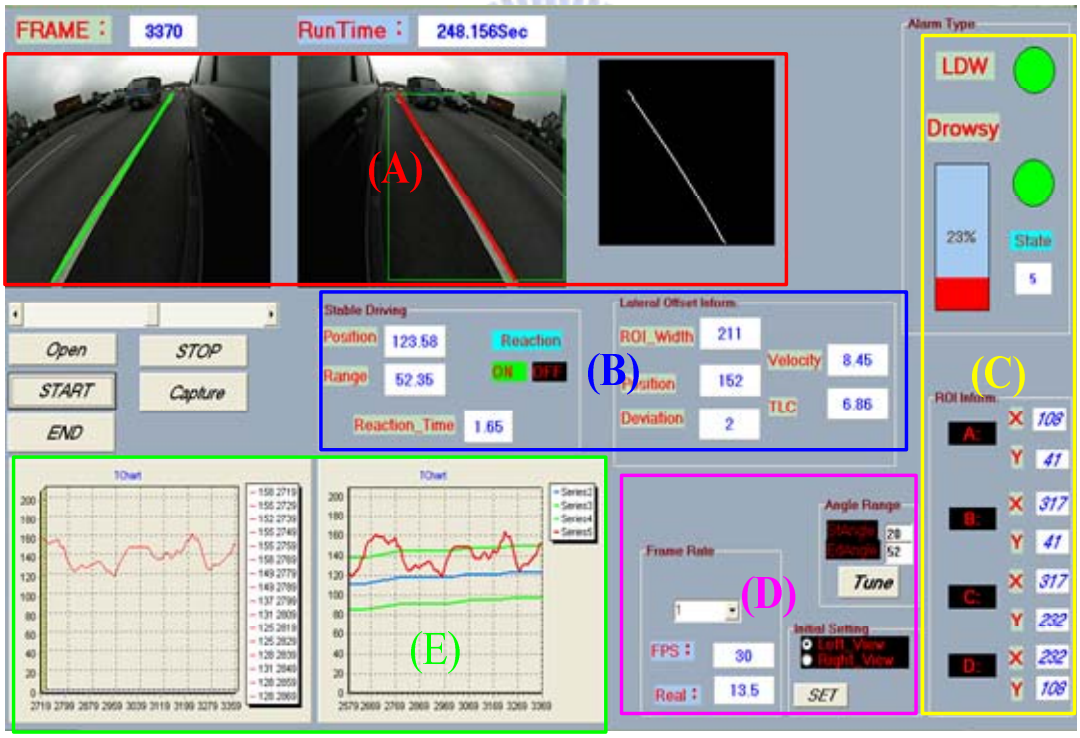

Fig. 5-2 : The programming interface in the PC platform.

Block (B) contains the display of the related lateral information computed by LDW system. Besides, it also shows the reaction time and stable-driving region, as

explained in Fig. 4-8. The warning alarms with different colors of lane of LDW and drowsiness estimation systems is contained by block (C), where the coordinate values about the border of ROI are also included. Block (D) shows the searching range of angles about the piece-wise edge linking model, as described in Section 3.4, and the output frame rate which responds to the systematic performance. At last, Block (E) records the lateral offset and the maximum and minimum range of the reconstructed stable-driving distribution with real-time update.

5.2 Results of Distinct Environments

5.2.1 Explanation of Experimental Conditions

The driving environment is focused on highway with different light conditions. The image sequences captured by the camera with unknown two pan- or tilt-angles are tested with the same lane detection algorithm in Fig. 5-3. At the same time, in order to observe if the lane-based warning system can maintain robust performance and tolerate the light variation, we select the video segments with three different periods, daytime, evening, and night of one day for experiment in the next section.

Fig. 5-3 : The testing image with different mounting angles.

5.2.2 Results of Lane Detection

In Fig. 5-4, the testing environment considers the two properties with respect to the view-angles and light conditions simultaneously. The detection results of daytime (a), evening (b), and night (c) are processed by the same programming setting.

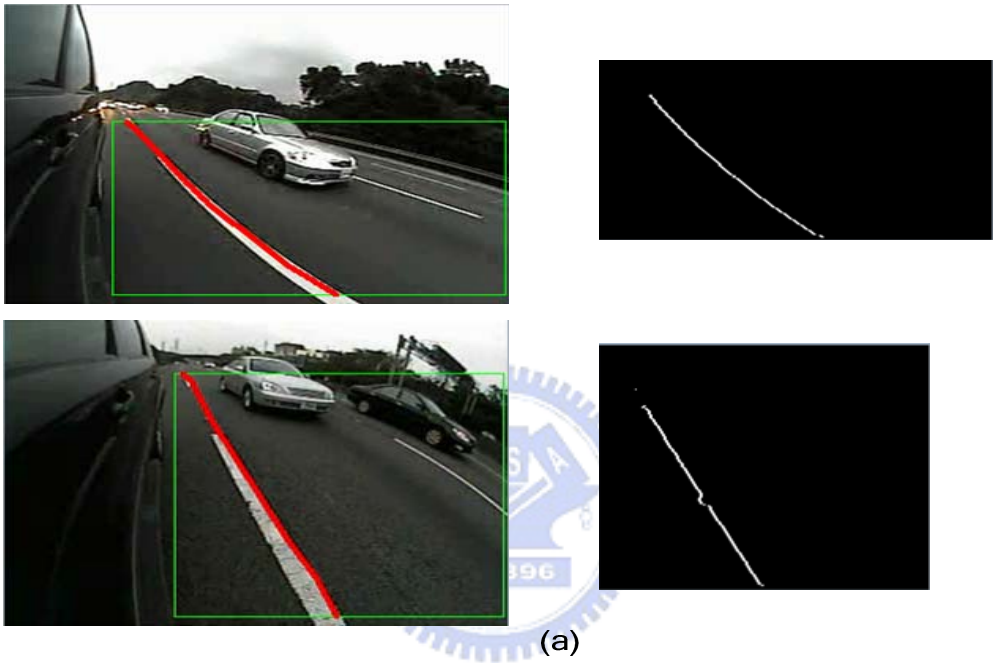

(a)

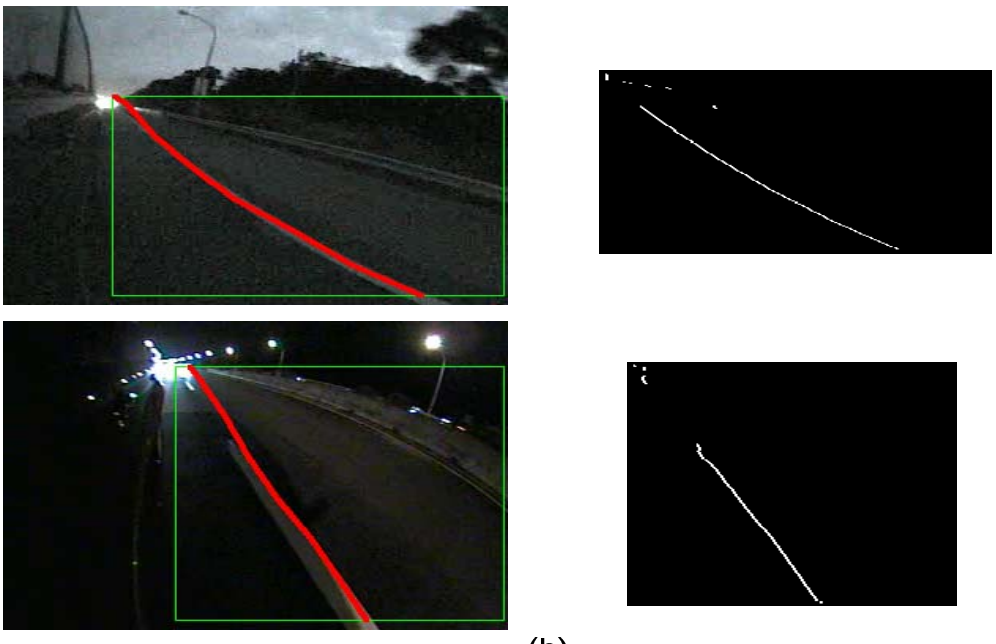

(b)

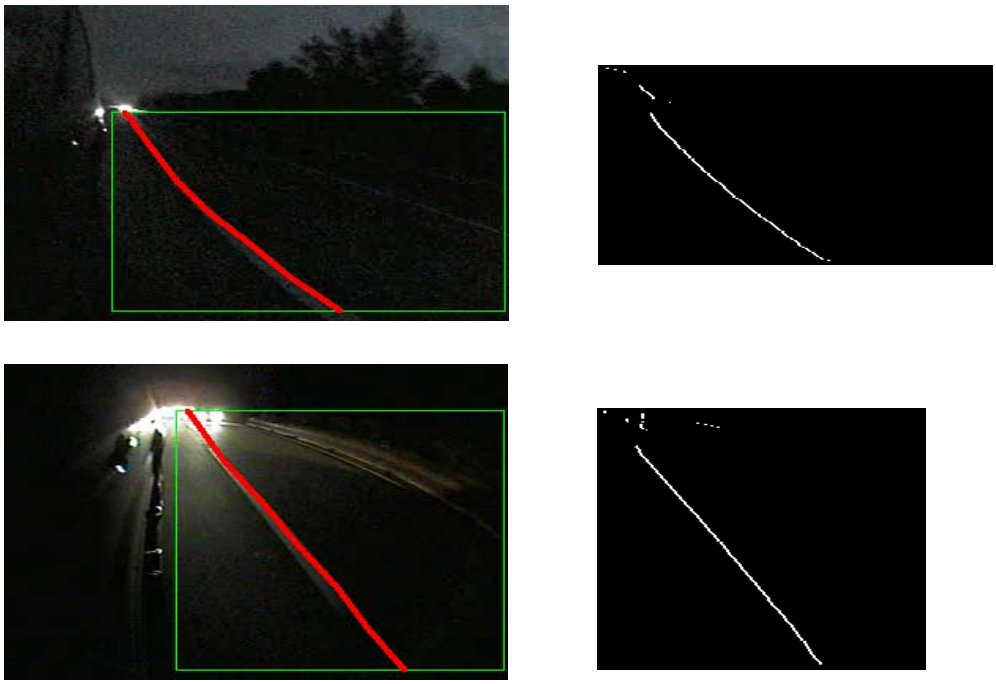

Fig. 5-4 : The results of lane detection.

In Fig. 5-4 (c), the lane boundary can be clearly extracted in the nighttime driving environment even if the side-view of vehicle usually has more chances to subject to the perturbation from the exterior light-sources.

5.2.3 Results of Lane Departure Warning

If the lane boundary is locked precisely by the lane detection mechanism, the lane departing maneuver can be tracked and recorded its position whether the lateral speed is faster or not. Figure 5-5, 5-6, and 5-7 shows the tracking results of lane departure with different variations of light and moving direction of the vehicle.

 # Frame 3293

 # Frame 3299

 # Frame 3305

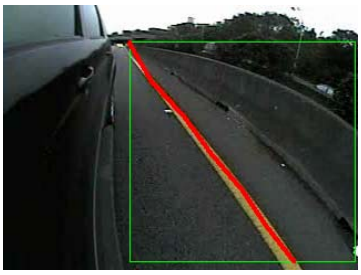

 # Frame 3310

 # Frame 3316

 # Frame 3334

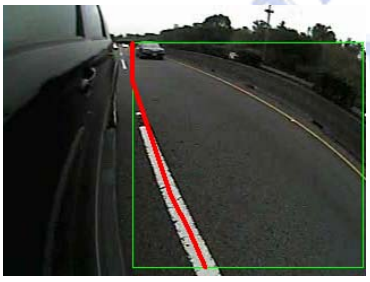

 # Frame 3385

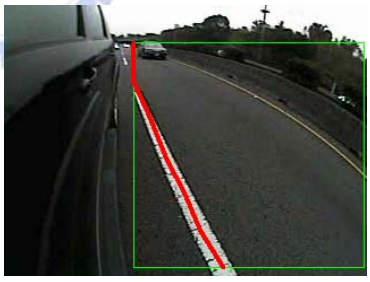

 # Frame 3388

Fig. 5-5 : The results of lane departure caused by cutting into the inside lane.

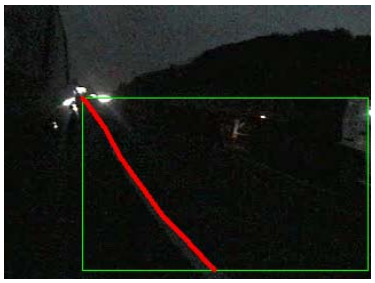

 # Frame 693

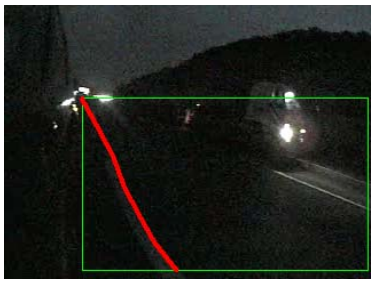

 # Frame 718

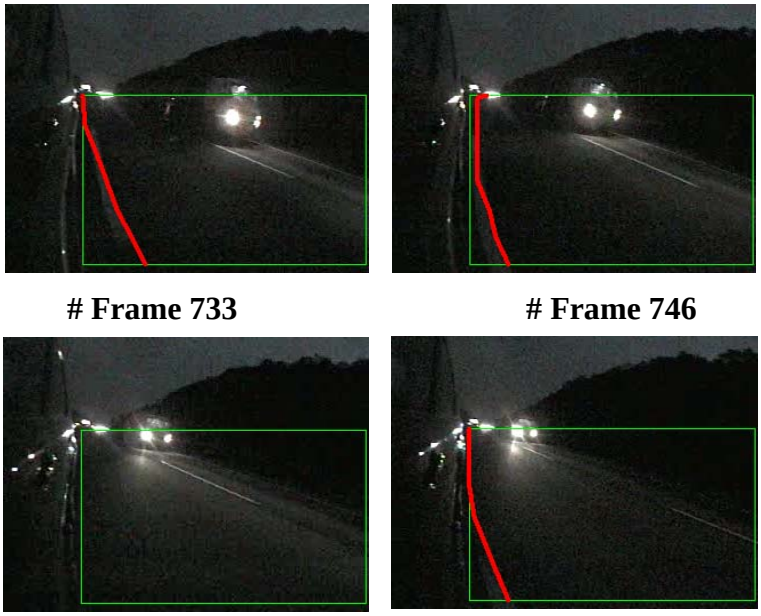

Fig. 5-6 : The results of lane departure in the night time.

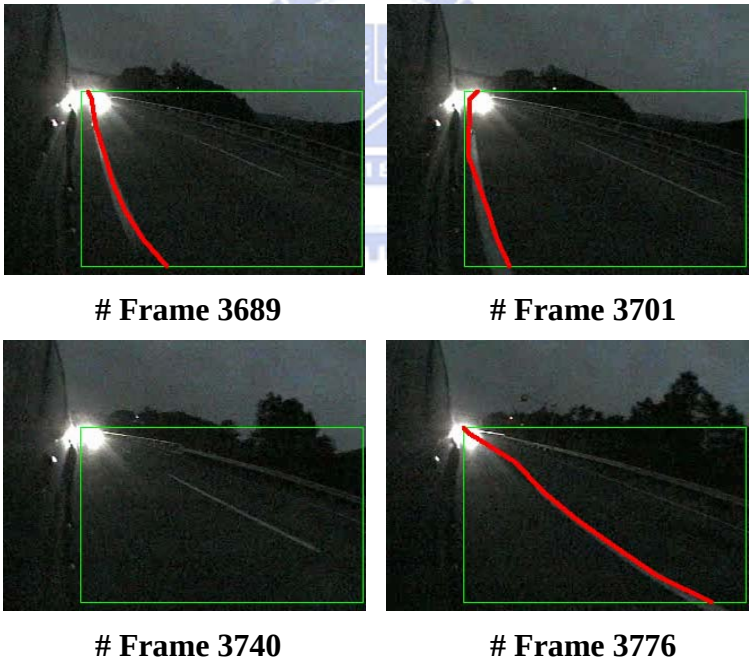

Fig. 5-7 : The results of lane departure caused by moving into the outside lane.

5.2.4 Results of Stable-Driving Region and Drowsiness Estimation System

As described in Section 4.3.3, the straight-road driving distance between the lane marker and wheels can be modeled by the clustered distribution with higher weight and smaller standard deviation. For further adaptation, we develop an update mechanism to make the stable region adaptive to the changeful driving habits of people. Figure 5-8 shows the updating process of stable-region described as a statistical chart which contains the information of lateral offsets at the same time. From Fig. 5-8 (a) to (d), the mean value of the stable-region will increase obviously due to the accumulated lateral offsets which are almost situated over the region and can be regarded as the new driving habit of the driver adequately.

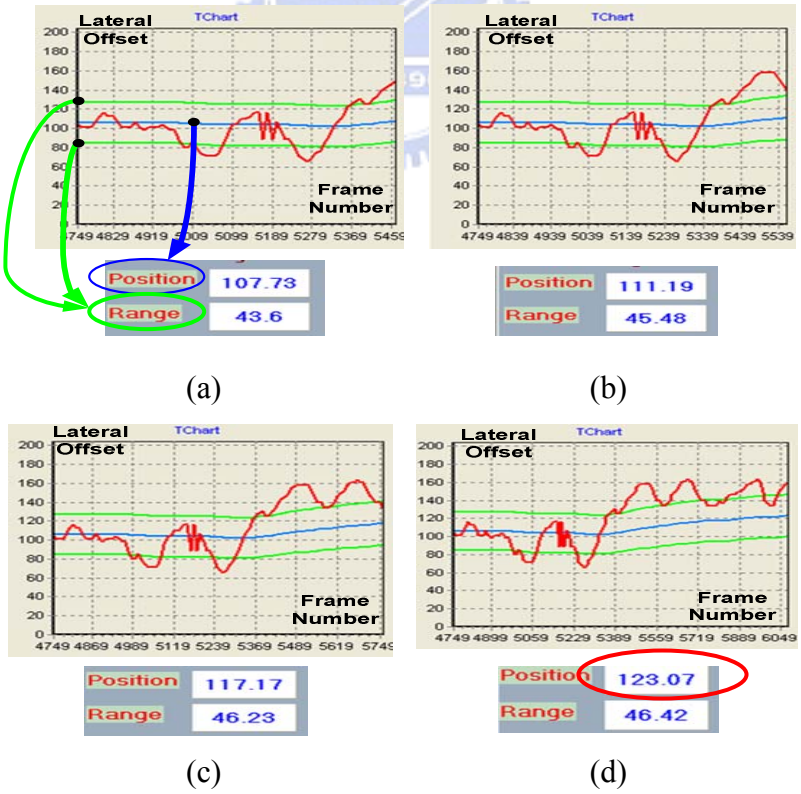

Fig. 5-8 : Results of update for the stable-driving region.

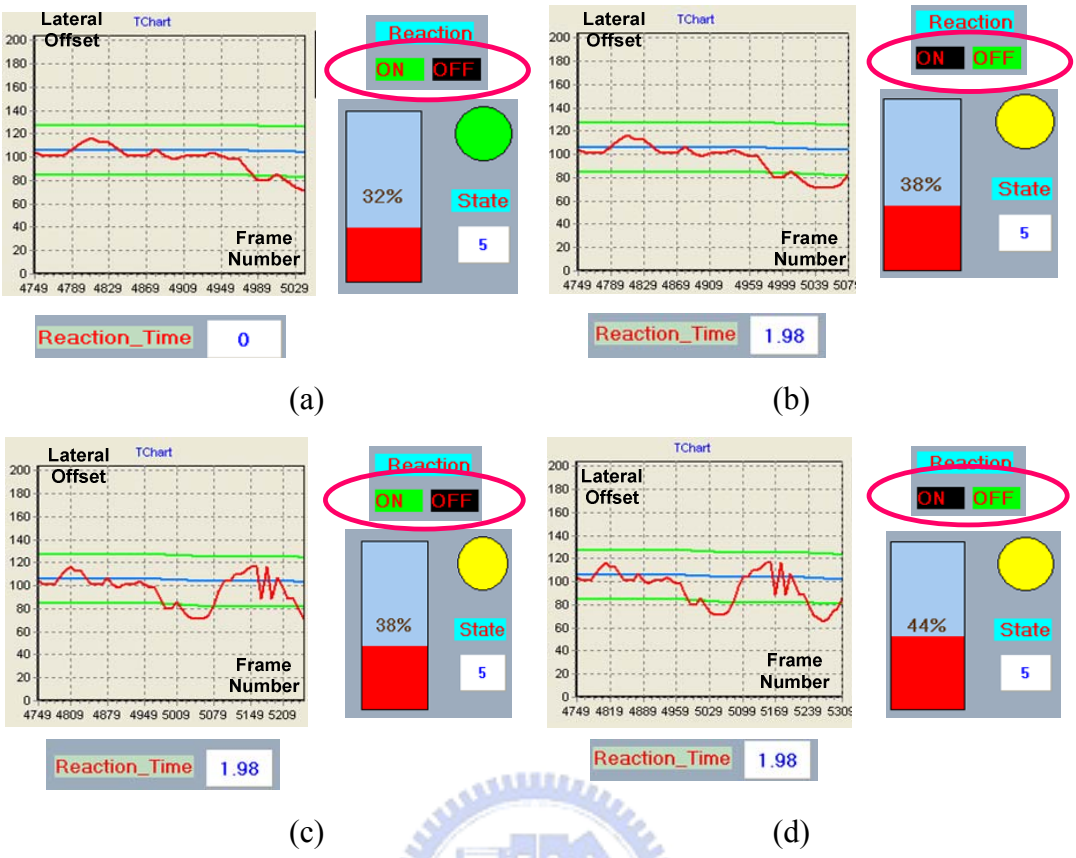

Fig. 5-9 : Results of the variation of drivers' drowsy degree by the reaction time.

The relationship between the gauge chart of drowsy degree and the reaction time of drivers is demonstrated in Fig. 5-9. From Fig. 5-9 (a) to (b), the reaction time will start to be counted since the lateral offset is outside the stable-region at that moment. Therefore, the drowsy degree can be raised with a specific ratio of the measured reaction time to the threshold which has been evaluated by the EGG-based analysis from BRC. On the other hand, from Fig. 5-9 (c) to (d), the drowsy degree keeps increasing because the time interval between the current and previous reaction time which are both greater than the threshold is not for 10 sec.

5.3 Performance

Table 6 : The processing information of lane detection algorithms.						
		Output FPS	ROI_size (width,height)	De-noise Processing (A) (%)	Lane Boundary Extraction (B) (%)	Piece-wise Edge Linking Model + LDWs (C) (%)
View1	Test1	**16.6**	**(245,146)**	**63%**	**24%**	**13%**
	Test2	**16.9**	**(250,142)**	**67%**	**24%**	**9%**
View2	Test1	**15.9**	**(204,194)**	**68%**	**16%**	**16%**
	Test2	**15.9**	**(204,200)**	**67%**	**15%**	**18%**

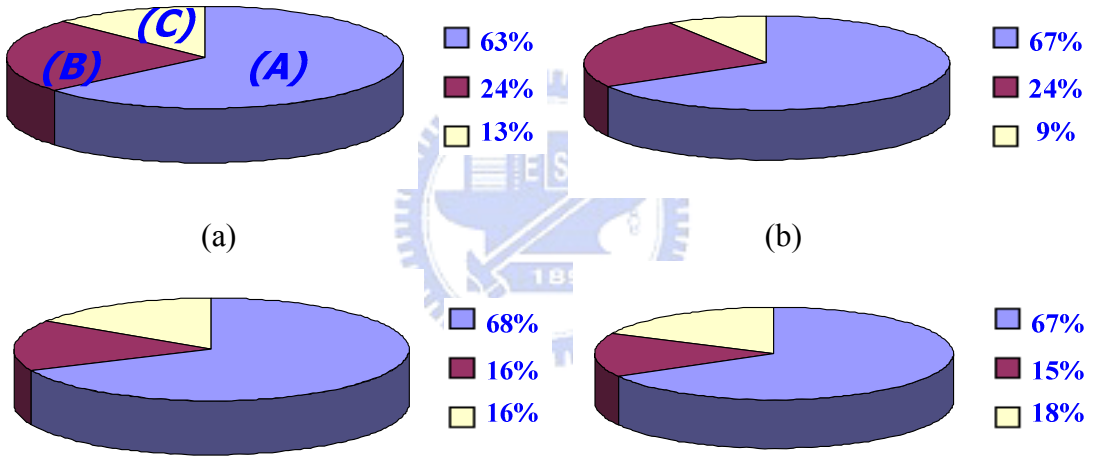

Fig. 5-10 : The processing ratio of 4 examples implemented by lane detection and lane departure warning algorithms.

The performance of the four testing videos with two different view-angles is listed in Table 6. We split the lane detection approach into three parts. (A): The de-noise preprocessing. (B): The lane boundary extraction. (C): The edge linking task and LDW. In general, the size of ROI has the most influence on the systematic execution time. However, the frequently departing maneuver occurred in the image

segments will result in the additional computing load. As explained in Section 3.4, the bottom sub-region of ROI must be searched for line-pixels with Hough Transform for each frame. In other words, the searching range in it can not be regarded as the limited size near the position determined by the previous lane marker if the lateral offsets change seriously. Figure 5-10 shows that the ratio of edge linking mechanism depends on the image contents whether the ROI is large or not. On the other hand, due to the 5x5 size of Gaussian mask, the de-noise procedure still occupies most of execution time even if the frequent departure exists or not.

5.4 Discussion and Analysis

In order to increase detection rate of LDW and drowsiness estimation system, the lane detecting error must be low as much as possible even if this algorithm is always subjected to the disturbance resulted from external factors. In Fig. 5-11, the lane markers can be still extracted by our developing method although they are unclear. However, the lane detection method we proposed in this thesis can not resolved some cases such as driving in a tunnel so that the contrast between lane markers and road surface is not enough, as shown in Fig. 5-12 (a).

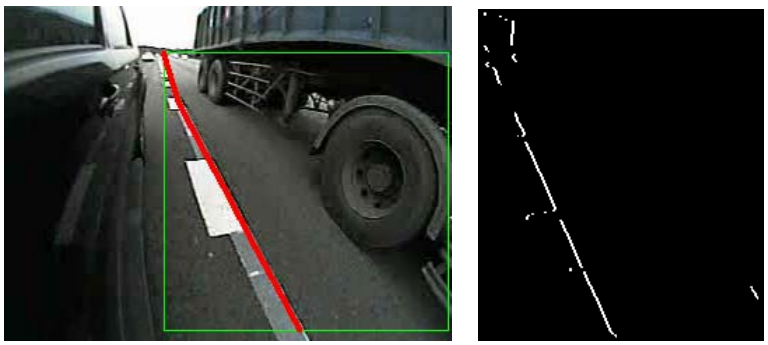

Fig. 5-11 : Results of lane detection for the unclear lane markers.

(a) (b)

(c)

Fig. 5-12 : Some examples of detecting error in our lane detection system.

In addition, as explained in Section 3.2, the range of ROI can be detected by the boundary information of the car window and that of the horizon in the image. But this property may be not suited to the environment which does not only contain the above clues for ROI extraction but be affected by the light conditions, such as the example shown in Fig. 5-12 (b). On the other hand, the external light in the nighttime has chance to produce a “light ring” effect on the camera lens which may cause the deviated parting position of the detected lane markers in the image instantaneously, as shown in Fig. 5-12 (c).

Chapter 6
Conclusions

We propose a scientific system for driver's drowsiness estimation by integrating the statistics evaluated by the EEG-based analysis from BRC into our lane departure warning system in the realistic driving environment. In this thesis of lane detection, we develop a method for automatic ROI extraction only by analyzing the image contents captured by the fish-eye camera mounted under the rear-view mirror without knowing the related camera parameters in advance. To overcome the light variations, the de-noising architecture which is considered the spatial and temporal domain at the same time can restrain the noise effectively. Focused on the geometric property of the blind-spot view, the adaptive type of edge operator and threshold selection can exactly detect the lane boundary. Finally, an improved edge linking model we proposed not only increases the searching speed for lane trajectory but resolves the effect of fish-eye lens distortion.

About the lane departure warning and drowsiness estimation proposed in this thesis, we construct a warning mechanism with the lateral offsets and TLC computed by the lateral velocity and the border of ROI. Due to the different driving habits of people, we construct the stable-driving region for modeling by the information of previous lateral positions of lane markers with updating mechanism. Then, we use the deviation as the index for drowsiness estimation which has been analyzed and evaluated by EEG-analysis. By considering the human's behavioral style that the reactive behavior must be increasingly slower for a long period when the subjects enter the drowsy state gradually, we design a gauge of drowsy degree to estimate the driver's psychological state according to the reaction time of drivers.

The lane-based stable system has been tested that the average frame rate is up to 15fps on PC platform. In the future, it will be integrated into the blind-spot side collision warning architecture to increase the better detection rate and provide more adaptive performance. Besides, by the constructed mechanism for drowsiness estimation in the dynamic driving environments, we can collect more data to further analyze the other inattentive behavior of drivers through this system so that the safety driving system can consider all the possible risks caused by the internal or external factors of drivers as much as possible.

References

[1] G. Jacobs, A. Aeron-Thomas, and A. Astrop, "Estimating global road fatalities," *Australian National University, Transport Research Laboratory, Technical Report TRL 445*, 1999.

[2] "Traffic safety facts 2004." *Technical report, National Center for Statistics and Analysis, U.S. Department of Transportation*, 2004.

[3] http://www.motc.gov.tw/hypage.cgi?HYPAGE=index.htm

[4] A. Broggi, M. Betozzi, A. Fascioli, C. Guarino, L. Bianco, and A. Piazzi, "The argo autonomous vehicle's vision and control systems," *Int'l Journal Intelligent Control and Systems*, vol. 3, no. 4, pp. 409-441, 1999.

[5] M. Bertozzi and A. Broggi, "GOLD: a parallel real-time stereo vision system for generic obstacle and lane detection," *IEEE Trans. Image Processing*, vol. 7, no. 1, Jan. 1998.

[6] G. Y. Jiang, T. Y. Choi, S. K. Hong ,J. W. Bae, and B. S. Song, "Lane and obstacle detection based on fast inverse perspective mapping algorithm," in *IEEE Conf. Systems, Man, and Cybernetics*, vol. 4, pp. 2969-2974, Oct. 2000.

[7] Y. Wang, D. Shen, and E. K. Teoh, "Lane detection using Catmull-Rom Spline," in *Proc. IEEE Intelligent Vehicles Symp.*, Stuttgart, Germany, pp. 51-57, 1998.

[8] Y. Wang, E. K. Teoh, and D. Shen, "Lane detection and tracking using B-Snake," *Image and Vision Computing,* vol. 22, pp. 269-280, 2004.

[9] C. R. Jung and C. R. Kelber, "A robust linear-parabolic model for lane following," in *Proc. SIBGRAOI, Curitiba, PR*, pp. 72-79, Oct. 2004

[10] C. C. Wang, S. S. Huang, and L. C. Fu, “Driver assistance system for lane detection and vehicle recognition with night vision”, in *Proc. IEEE Intelligent Robots and Systems*, pp. 3530-3535, Aug. 2005.

[11] R. Risack, N. Mohler, and W. Enkelmann, “A video-based lane keeping assistant”, in *Proc. IEEE Intelligent Vehicles Symp.*, Dearborn, MI, pp. 506-511, Oct. 2000.

[12] S. Y. Kim and S. Y. Oh, “A driver adaptive lane departure warning system based on image processing and a fuzzy evolutionary technique,” in *Proc. IEEE Intelligent Vehicles Symp.*, Columbus, OH, pp.361-365, Jun. 2003.

[13] K. Weiss, N. Kaempchen, and A. Kirchner, “Multiple-model tracking for the detection of lane change maneuvers,” in *Proc. IEEE Intelligent Vehicles Symp.*, Parma, Italy, pp. 937-942, 2004.

[14] W. Enkelmann, “Video-based driver assistance-from basic functions to applications,” in *Proc. Int’l Journal Computer Vision*, vol. 45, no. 3, pp. 201-221 , Dec. 2001.

[15] P. H. Batavia, “Driver-adaptive lane departure warning systems,” ***doctoral dissertation,*** Robotics Institute, Carnegie Mellon University, Sep. 1999.

[16] R. Kovordanyi, “Dynamically deployed support as a potential solution to negative behavior adaptation,” in *Proc. IEEE Intelligent Vehicles Symposium*, pp. 613-618, 2005

[17] 林亨杰, ”高速公路速限提昇前後之交通事故探討,” *道路交通安全與執法國際研討會*, Sep. 2004.

[18] M. J. Flannagan, “Current status and future prospects for non-planar rearview mirrors” in *SAE Technical Paper Series No. 2000-01-0324*

[19] 席世民, “學校交通安全教育工作推動現況與基本安全觀念介紹,” *交通部道路交通安全督導委員會*, Aug. 2004

[20] C. Kreucher and S. Lakshmanan, "LANA: A lane extraction algorithm that uses frequency domain features," *IEEE Trans. Robotics and Automation*, vol. 15, no. 2, Apr. 1999.

[21] Y.-U. Yim and S.-Y. OH, "Three-feature based automatic lane detection algorithm (TFALDA) for autonomous driving," *IEEE Trans. Intelligent Transportation Systems,* Vol. 4, NO. 4, Dec. 2003.

[22] Q. Li, N. Zheng, and H. Cheng, "Springrobot: a prototype autonomous vehicle and its algorithms for lane detection," *IEEE Trans. On Intelligent Transportation Systems,* Vol. 5, NO. 4, Dec. 2004.

[23] M. Chen, T. Jochem, and D. Pomerleau, "AURORA: a vision-based roadway departure warning system," *in Proc. IEEE Int'l Conf. Intelligent Robots and Systems,* vol. 1, pp. 243-248, Aug. 1995

[24] C.-H. Yeh and Y.-H. Chen, "Development of vision-based lane and vehicle detecting systems via the implementation with a dual-core DSP," in *Proc. IEEE Intelligent Transportation Systems Conf.,* Sep. 17-20, 2006.

[25] R. Chapuis, R. Aufrere, and F. Chausse, "Accurate road following and reconstruction by computer vision," *IEEE Trans. Intelligent Transportation Systems,* vol. 3, no. 4, Dec. 2002.

[26] J. W. Lee, "A machine vision system for lane-departure detection," in *Proc. Computer Vision and Image Understanding,* vol. 86, pp. 52-78, Apr. 2002.

[27] C.-T. Lin, R.-C. Wu, S.-F. Liang, W.-H. Chao, Y.-J. Chen, and T.-P. Jung, "EGG-based drowsiness estimation for safety driving using independent component analysis," *IEEE Trans. Circuits and Systems,* vol.52, Dec. 2005.

[28] A. Lopez, C. Canero, J. Serrat, J. Saludes, F. Lumbreras, and T. Graf, "Detection of lane markings based on ridgeness and RANSAC," in *Proc. IEEE Conf. on Intelligent Transportation Systems,* pp.254-259, Sep. 13-16, 2005.

[29] C. R. Jung and C. R. Kelber, "A lane departure warning system using lateral offset with uncalibrated camera," in *Proc. IEEE Conf. on Intelligent Transportation Systems,* pp. 102-107, Sep. 13-16, 2005.

[30] D. J. Kang, J. W. Choi, and I. S. kweon, "Finding and tracking road lanes using line-snakes", in *Proc. IEEE Conf. on Intelligent Vehicles Symposium,* pp. 189-194, Sep. 1996

[31] M. Ruder, W. Enkelmann, R. Garnitz, "Highway lane change assistant," in *Proc. IEEE Conf. on Intelligent Vehicles Symposium,* Vol.1, pp.240-244, Jun. 2002.

[32] C. Stauffer, W.E.L Grimson, "Adaptive background mixture models for real-time tracking," in *Proc. IEEE Computer Society Conference on Computer Vision and Pattern Recognition,"* Vol.2, 1999.

[33] R. K. Lenz and R. Y. Tsai, "Techniques for calibration of the scale factor and image center for high accuracy 3-D machine vision metrology," *IEEE Trans. On Pattern Analysis and Machine Intelligence,* Vol.10, NO. 5, Sept. 1988.

[34] R.I. Hartley and S. B. Kang, "Parameter-tree radial distortion correction with centre of distortion estimation," in *Proc. IEEE International Conf. On Computer Vision,* Vol.2, pp. 1834-1841, Oct. 2005.

[35] H. Godthel, P. Milgram, and G. J. Blaauw, " The development of a time-related measure to describe driver strategy," *Human Factors,* 26(3): 257-268, 1984.

[36] P. Philip, J. Taillard, "Effect of fatigue on performance measured by a driving simulator in automobile drivers," *Journal Psychosomatic Research* 55, pp. 197-200, 2003.

[37] J. Hendrix, "Fatal crash rates for tractor-trailers by time of day," in *Proc. Int'l Truck and Bus Safety Research and Policy Symp.,* pp. 237-250, 2002.